Journal of Asian Earth Sciences 70–71 (2013) 265–282

Contents lists available at SciVerse ScienceDirect

Journal of Asian Earth Sciences

journal homepage: www.elsevier.com/locate/jseaes

Provenance of lateritic bauxite deposits in the Wuchuan–Zheng'an–Daozhen area, Northern Guizhou Province, China: LA-ICP-MS and SIMS U–Pb dating of detrital zircons

Jing Gu [a,b], Zhilong Huang [a,*], Hongpeng Fan [a,b], Lin Ye [a], Zhongguo Jin [c]

[a] State Key Laboratory of Ore Deposit Geochemistry, Institute of Geochemistry, Chinese Academy of Sciences, 46 Guanshui Road, Guiyang 550002, China
[b] University of Chinese Academy of Sciences, Beijing 100049, China
[c] Guizhou Nonferrous Metal and Nuclear Industry Geological Exploration Bureau, Guiyang 550005, China

ARTICLE INFO

Article history:
Received 26 November 2012
Received in revised form 5 March 2013
Accepted 18 March 2013
Available online 28 March 2013

Keywords:
Bauxite deposit
Detrital zircons
Yangtze Block
Cathaysia Block
Provenance
Wuchuan–Zheng'an–Daozhen area

ABSTRACT

The provenance of the large and super-large scale bauxite deposits developed in the Wuchuan–Zheng'an–Daozhen (WZD) alumina metallogenic province in the Yangtze Block of South China is poorly understood. LA-ICP-MS and SIMS U–Pb dating of detrital zircons from bauxite ores and the underlying Hanjiadian Group in the WZD area provide new constrains on the provenance of the WZD bauxite and provide new insight on the bauxite ore-forming process. The ages of the detrital zircons in the bauxites and the zircons in the Hanjiadian Group are similar suggesting that the bauxites are genetically related to the Hanjiadian sediments. The detrital zircon populations of the four samples studied show four primary age peaks: 2600–2400 Ma, 1900–1700 Ma, 1300–700 Ma and 700–400 Ma. The age distribution of detrital zircons indicates that they are probably derived from various sources including Neoproterozoic, Mesoproterozoic, Paleoproterozoic, Archean and some minor Paleozoic sources. The most abundant age population contains a continuous range of ages from 1300 to 700 Ma, ages consistent with subduction-related magmatic activities (1000–740 Ma) along the western margin of the Yangtze Block and the worldwide Grenville orogenic events (1300–1000 Ma). Thus, it is suggested that the main provenances of the WZD bauxite and the Hanjiadian Group are the Neoproterozoic igneous rocks in the western Yangtze Block and the Grenville-age igneous rocks in the southern Cathaysia Block. In addition, this work verifies that the global Grenville orogenic events and subduction-related magmatic activities associated with the Yangtze Block had a significant influence on the formation of the WZD bauxite deposits.

1. Introduction

Bauxite deposits are commonly classified into two main categories: karstic bauxite overlying carbonate rocks and lateritic bauxite which overly aluminosilicate rocks (Bárdossy, 1982). The geochemistry, precursor lithologies, genetic implications and ore-forming processes related to karst bauxite deposits in the world have been investigated by numerous authors (e.g. Bárdossy, 1982; Bárdossy and Kovács, 1995; MacLean et al., 1997; Liaghat et al., 2003; Calagari and Abedini, 2007; Taylor et al., 2008; Karadag et al., 2009; Dariush Esmaeily et al., 2010; Deng et al., 2010; Liu et al., 2010a; Zarasvandi et al., 2008, 2010), whereas lateritic bauxites have rarely been studied (e.g. Bárdossy and Aleva, 1990; Boulange B, 1990; Schwarz, 1997). Although most lateritic bauxites are derived directly from the underlying source rocks and have textures and compositions similar to their parent lithology (e.g. Horbe and da Costa, 1999; Mutakyahwa et al., 2003), the depositional source of bauxite and the source rocks in some cases be difficult to determine because of the influence of complex tectonic movements that occurred after the bauxite ore deposits were formed.

Bauxite resources in China are abundant, ranking fifth in the world, after Guinea, Australia, Brazil, and Jamaica (Liu et al., 2010a). The North Guizhou Province in the Yangtze Block (Fig. 1) comprises a series of lateritic bauxite deposits and is an important resource base for bauxite in China. In the last 3 years, huge quantities of lateritic bauxite ores have been discovered in Wuchuan, Zheng'an and Daozhen Counties, Northern Guizhou. Mineral exploration and a series of research studies have recently been carried out in the Wuchuan–Zheng'an–Daozhen (WZD) region by the Guizhou Nonferrous Metal Geological Exploration Bureau and the Bureau of Geology and Mineral Exploration and Development of Guizhou Province. More than 20 lateritic bauxite deposits (Fig. 2) with more than 100 million tons of bauxite reserves have been identified in the area and several other unexplored districts also

* Corresponding author. Tel.: +86 851 5895900; fax: +86 851 5891664.
E-mail address: huangzhilong@vip.gyig.ac.cn (Z. Huang).

1367-9120/$ - see front matter © 2013 Elsevier Ltd. All rights reserved.
http://dx.doi.org/10.1016/j.jseaes.2013.03.018

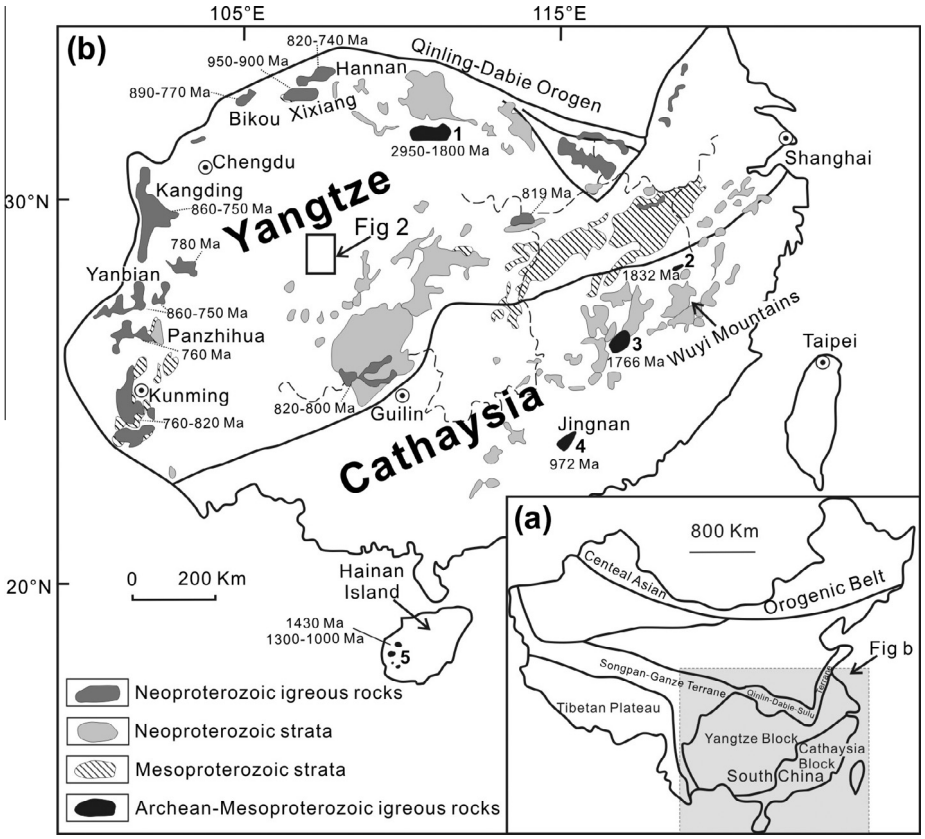

Fig. 1. (a) Tectonic framework of China showing the location of the South China Block; (b) distribution of the Precambrian igneous rocks and strata in South China (modified after Zheng et al., 2007). Numbers 1–5 indicate the Kongling Complex, the Danzhu gneissic granite, the Tianjingping amphibolite, the Jingnan rhyolites, and the Baoban complex, respectively.

show bauxite mineralization potentials. Initial investigations have provided a first insight into the geology, geochemistry and conditions of bauxite deposits formation in the WZD area (e.g. Liu, 2007; Wu et al., 2006, 2008a; Jin et al., 2009; Yin, 2009; Liu et al., 2010b; Gu et al., 2011).

Age constraints on the WZD bauxites are provided by the stratigraphic age of the underlying and overlying strata (e.g. Chen et al., 1987; Liao, 1988; Liang, 1989; Liu, 1995, 2007; Wu et al., 2006; Hao et al., 2007; Zhao and Wang, 2008)). The limestones above the bauxites are Middle Permian (the Qixia Formation) and the bauxite horizons are underlain by Upper Carboniferous limestones (the Huanglong Formation). However, despite the reasonably well-defined stratigraphic framework, the origin of these bauxites remains controversial (Wu et al., 2006, 2008a; Jin et al., 2009; Gu et al., 2011). Based on comparisons of the rare earth element (REE) patterns and ratios of immobile elements, the underlying Silurian Hanjiadian Group, stratigraphically below the Huanglong Formation, is considered to be the major source rock for the bauxites (Jin et al., 2009; Gu et al., 2011). However, conclusions reached by precursor studies like these are often problematic because of the complex effects of lateritic weathering and post-bauxitization diagenesis. Therefore, more focused research is needed to (1) identify whether the underlying Hanjiadian Group is the source rock for the bauxite; (2) determine the provenance (depositional source) of the sediments that make up the Hanjiadian Group and the bauxite, and (3) provide details on the ore-forming process.

Detrital zircon, a ubiquitous heavy mineral in sedimentary rocks, can survive erosion, transport, diagenesis, and metamorphism and the age distribution of a large number of detrital zircons can reflect the age of the zircon bearing source rocks. Therefore, U–Pb detrital zircon geochronology can be a powerful tool for determining the provenance of sedimentary rocks and has been successfully applied worldwide (e.g., Fedo et al., 2003; Najman, 2006; Newson et al., 2006; Deng et al., 2010; Long et al., 2010; Jiang et al., 2011; Pereira et al., 2012). U–Pb ages of zircons in bauxites provide direct evidence for the age and origin of the potential parent rock and thus indicate the provenance of the bauxite ores (e.g., Deng et al., 2010). In this paper, we report secondary ion mass spectroscopy (SIMS) and laser ablation inductively coupled plasma mass spectrometry (LA-ICP-MS) U–Pb ages for detrital zircons from two bauxite samples and two samples from the Hanjiadian Group to answer the progenitor, provenance, and ore-forming process questions enumerated above but also to help identify other prospects for bauxite in the WZD area and other nearby unexplored districts.

2. Geological setting

The South China Block consists of the Yangtze Block in the northwest and the Cathaysia Block in the southeast. The Yangtze Block is separated from the North China Block to the north by the Qinlin-Dabie-Sulu Orogen, is bounded by the Tibetan Plateau to the southwest, and the Cathaysia Block to the southeast (Fig. 1a). The Cathaysia Block is dominated by Phanerozoic igneous rocks (especially Mesozoic granitoids) and sedimentary rocks with sparsely exposed Precambrian metamorphic units (Yu et al., 2010). Most of the Precambrian metamorphic rocks in this area were thought to be Paleo-Mesoproterozoic and some even Neoarchean in age (Hu et al., 1991; Hu, 1994; Gan et al., 1995; Li, 1997; Zhuang et al., 2000). However, many of these rocks have recently been demonstrated to have formed in the Neoproterozoic and even later

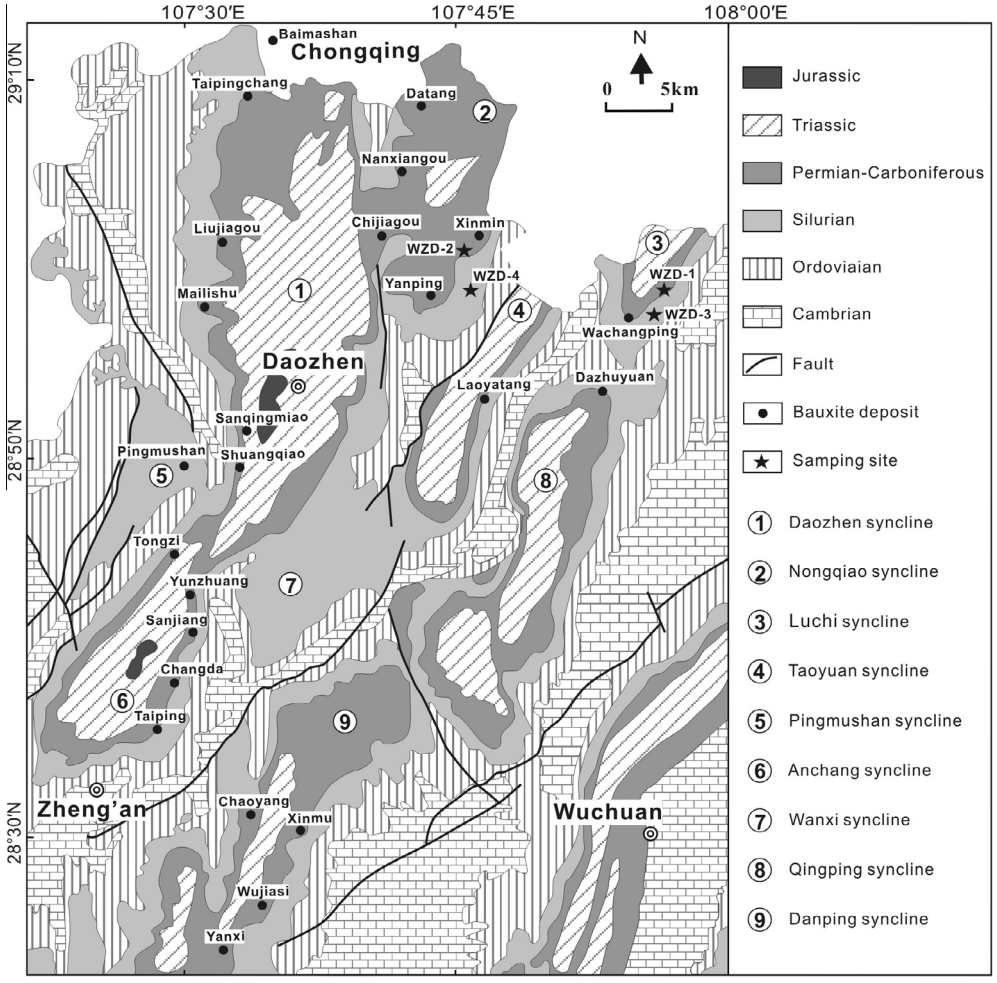

Fig. 2. Simplified geological map of the bauxite deposits in the WZD area (modified after Wu et al., 2008a).

(Li et al., 2005, 2010a,b; Yu et al., 2005, 2010, 2012; Wan et al., 2007); the Archean ages obtained by the Sm–Nd isochron method are probably unreliable (e.g., Li, 1997). There are two known Paleoproterozoic igneous rocks: the 1832 ± 6 Ma Danzhu gneissic granite (marked as "2" in Fig. 1b) in the northern Cathaysia Block (SHRIMP U–Pb zircon, Li and Li, 2007), and the 1766 ± 19 Ma protolith age for the Tianjingping amphibolite (marked as "3" in Fig. 1b) (SHRIMP U–Pb zircon, Li, 1997). Mesoproterozoic igneous rocks are represented by the ca. 980 Ma Jingnan rhyolites (marked as "4" in Fig. 1b) in the southwestern Wuyi Mountains (Shu et al., 2008a,b) and the ca. 1430 Ma Baoban gneissic granitoids (marked as "5" in Fig. 1b) that were metamorphosed at 1300–1000 Ma in the Hannan Island (Li et al., 2002b) (Fig. 1b).

The Yangtze Block is mainly composed of a Mesoproterozoic basement sequence and Neoproterozoic to Triassic cover sequences (e.g., Fan et al., 2013). Paleoproterozoic to Archean rocks crop out at only a few localities in the Yangtze Block. The oldest rocks reported in the Yangtze Block belong to the 2950 Ma Kongling complex (marked as "1" in Fig. 1b) in the northern part of the block (Qiu and Gao, 2000; Zhang et al., 2006a; Jiao et al., 2009). The Kongling complex consists of Archean to Paleoproterozoic high-grade metamorphic TTG (tonalite, trondhjemite and granodiorite) gneisses, metasedimentary rocks and amphibolites (e.g., Qiu and Gao, 2000). The existence of Archean basement and even a Paleoarchean (3500 Ma) continental nucleus beneath the Yangtze Block has been recognized by many researchers through the U–Pb geochronology and the Hf isotope composition of xenocrystic and inherited zircons (Zhang et al., 2006b,c; Zheng et al., 2006). Zhao et al. (2010) and Wang et al. (2012) reached the same conclusion based on detrital zircon analyses of Paleo- to Neoproterozoic sedimentary rocks in the southwestern Yangtze Block. In addition, 2030–1970 Ma granulites and 1850 Ma A-type granites and mafic dykes have been identified in the northern part of the Yangtze Block (the Kongling Complex; Fig. 1b) (Zhang et al., 2006b; Sun et al., 2008a; Wu et al., 2008b; Xiong et al., 2009; Peng et al., 2009, 2012). The Mesoproterozoic basement sequence is represented by the Kunyang, Huili, and Sibao Groups. Neoproterozoic strata include volcanic–sedimentary sequences known as the Yanbian, Suxiong, Danzhou, and Bikou Groups. Latest Mesoproterozoic to Neoproterozoic (ca. 1050–740 Ma) igneous rocks are widespread along the western margin of the Yangtze Block (Li et al., 2006). Among them, mid-Neoproterozoic granites, mafic rocks and sedimentary rocks ranging in age from 860 to 740 Ma predominate, mainly along the margins of the Yangtze Block (Li et al., 2002a; Zhou et al., 2002b) (Fig. 1b). In addition, there are rare minor igneous rocks older than 860 Ma (mostly older than 900 Ma) exposed along the western and southeastern margin of the Yangtze Block (Li et al., 2006).

The WZD area is located near the southern margin of the Yangtze Block (Fig. 1b). The exposed stratigraphic sequence in this area mainly consists of Cambrian, Ordovician, Silurian, Carboniferous, Permian, Triassic, Jurassic, and Quaternary units (Fig. 2). During Cambrian to Middle Silurian time, the region experienced a large transgression–regression cycle influenced by the initial stage of Caledonian movement. This transgression–regression cycle resulted in the deposition of Cambrian to Silurian strata in the

WZD area (Guizhou Provincial Geological Survey Bureau, 1987). The oldest rock in the area is the Middle to Upper Cambrian dolomite of the Loushanguan Group (Fig. 3). The Ordovician consists of dolomite, limestone and argillite and is overlain by the lower-Middle Silurian Hanjiadian Group, which is composed of grayish-green or fuchsia shales with intercalated sandstones and siltstones. During Upper Silurian to Upper Carboniferous time, a drop in sea level led to an epeirogenic phase that exposed the Hanjiadian Group to intense weathering (Guizhou Provincial Geological Survey Bureau, 1987). There are no outcrops of Upper Silurian, Devonian or Lower to Middle Carboniferous sediments in the area. The Upper Carboniferous limestone of the Huanglong Formation is mostly eroded and crops out only at a few localities in the region. During the Lower to Middle Permian, in situ weathering zones developed on the Hanjiadian Group and, after slight uplift, it was subjected to severe lateritic weathering again under warm humid climatic conditions resulting in the formation of the WZD bauxite deposits. The bauxitic–lateritic horizons are overlain by the Middle Permian limestone of the Qixia and Maokou Formations. Coal-rich Triassic units overlying the bauxite (dolomite, limestone, shale and sandstone) are in turn overlain by Jurassic shales and sandstones.

Because of NNE-directed compression in this region, NNE-trending anticlines, synclines and faults are ubiquitous (Fig. 2). The bauxitic horizons, usually cut by faults and fractures, are strictly controlled by synclines. Moreover, the ores are all hosted in limbs of the synclines (Fig. 2).

3. Sampling and analytical methods

Four representative samples, two bauxite samples (WZD-1, WZD-2) and two samples of the Hanjiadian Group (WZD-3, WZD-4) were collected from the WZD area. Sample locations are shown in Fig. 2. Zircon grains were separated from the four samples using conventional heavy liquid and magnetic techniques and then mounted in epoxy resin and polished down to expose the grain centers. Cathodo-luminescence (CL) photos (Fig. 4) were acquired with a Mono CL3+(Gatan, USA) attached to a scanning electron microscope (Quanta 400 FEG) at the State Key Laboratory of Continental Dynamics, Northwest University, Xi'an.

U–Pb zircon dating of sample (WZD-1) was conducted using a Cameca IMS 1280 ion microprobe (SIMS) at the Institute of Geology and Geophysics, the Chinese Academy of Sciences (CAS) in Beijing. Details of the analytical procedures for zircon U–Pb dating have previously been reported (Li et al., 2009, 2010a,b). The uncertainties in ages are cited as 1σ, and the weighted mean ages are quoted at the 95% confidence interval (2σ). The SIMS U–Pb detrital zircon data is presented in Table 1. U–Pb zircon dating of the other three samples (WZD-2, WZD-3 and WZD-4) was carried out at the State Key Laboratory of Continental Dynamics, Northwest University, Xian, China. The ICP-MS instruments used were an ELAN6100 DRC from Perkin Elmer/SCIEX (Canada) with a dynamic reaction cell (DRC) and an Agillent 7500a. A GeoLas 193 nm laser-ablation system was used for the laser-ablation analyses. The diameter of the analytical spot was 30 μm. The depth of these ICP-MS analyses is probably about 20–40 μm. Details of the analytical technique are given in Yuan et al. (2008). All U–Th–Pb isotope measurements were performed using zircon 91500 as an external standard for age calculation (Wiedenbeck et al., 1995) and NIST SRM 610 as the external standard for the concentration calculation in conjunction with the internal standardization ^{29}Si (32.8% Si in zircon). Common lead correction was carried out using the EXCEL program ComPbCorr#151 (Andersen, 2002). The age computations and

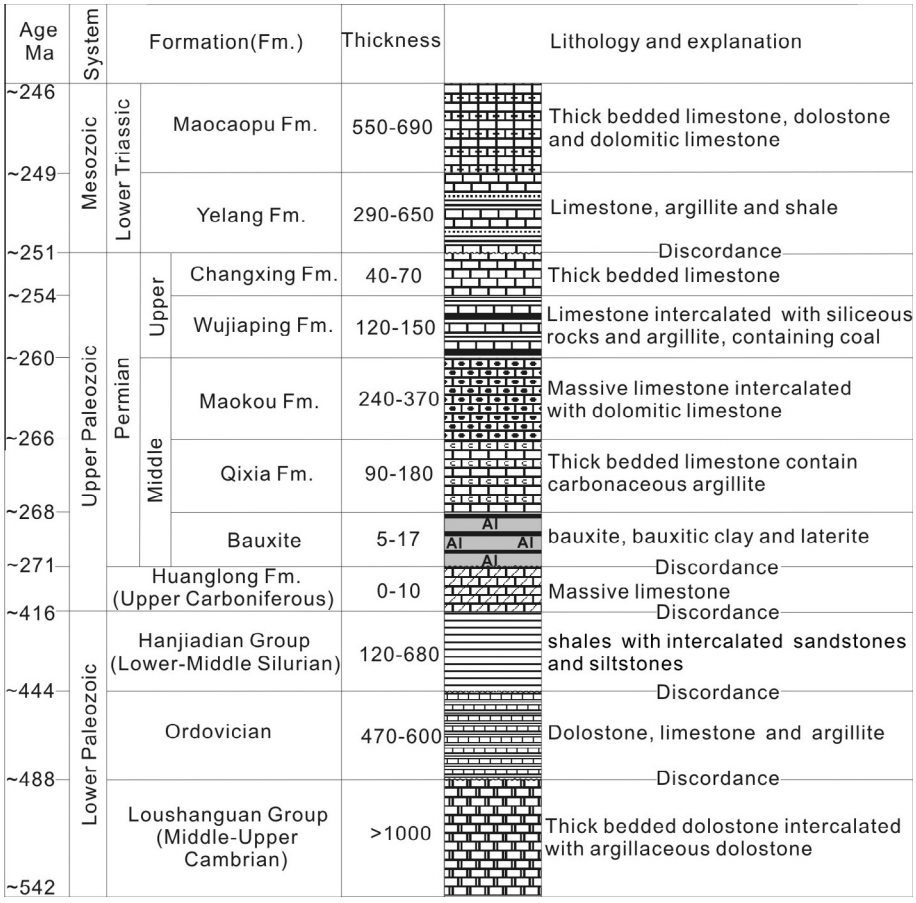

Fig. 3. Stratigraphic columnar section of the study area.

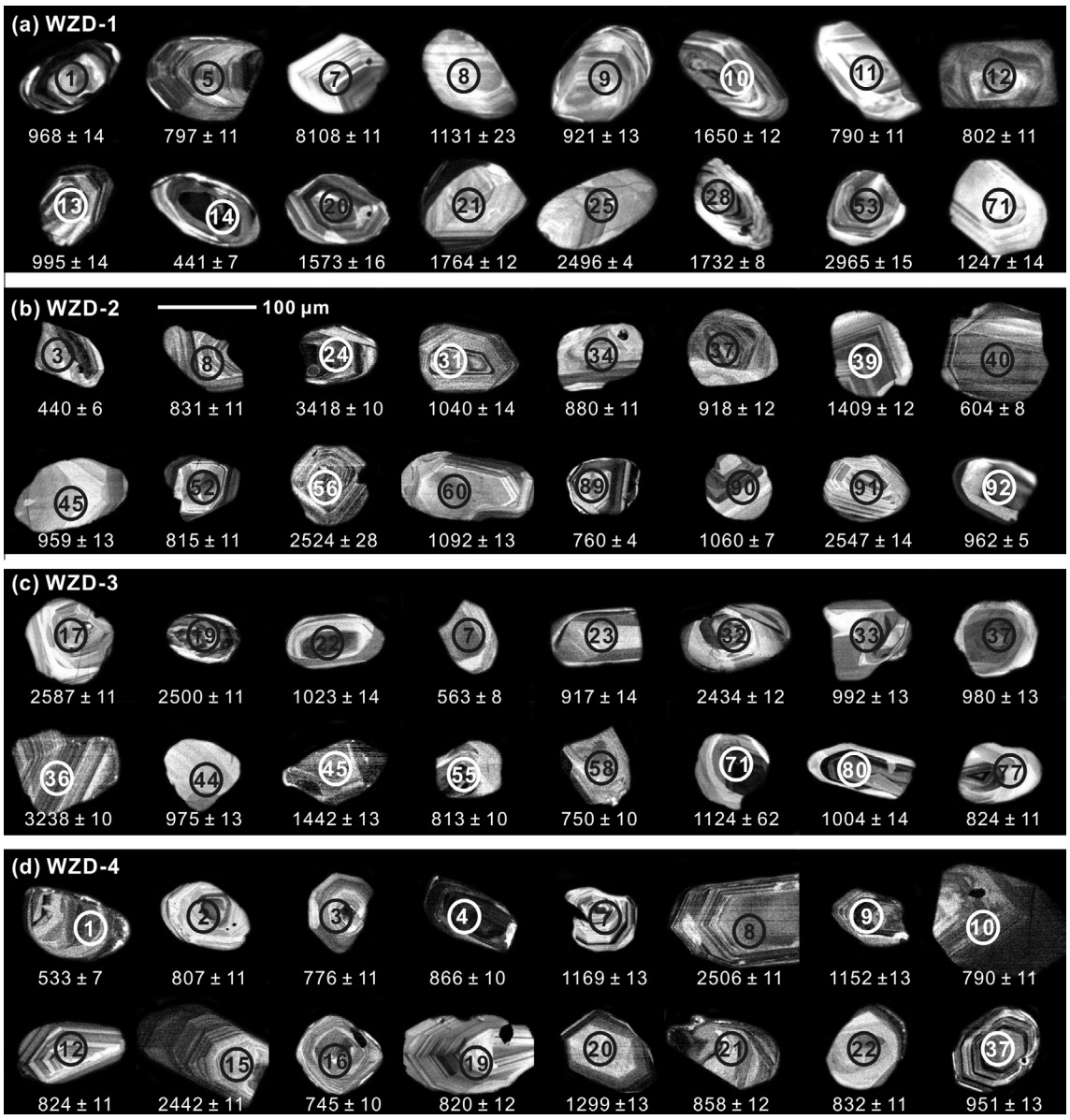

Fig. 4. CL images of detrital zircons from the studied samples.

concordia diagrams were done using the ISOPLOT (version 3.0) (Ludwig, 2003). Unless otherwise stated, the age data shown in the figures and subsequent discussions are based on $^{207}Pb/^{206}Pb$ ages for grains older than 1.0 Ga, and $^{206}Pb/^{238}U$ ages for younger grains. Zircon U–Pb isotopic compositions are presented in Table 2. Uncertainties on individual analyses in the data table and concordia plots are presented as 1σ.

4. Results

4.1. Bauxite samples WZD-1 and WZD-2

Detrital zircon grains show a wide range in size and morphology (Fig. 4). The zircon population of samples WZD-1 and WZD-2 are dominated by medium sized grains (60–120 μm; 80%) but also includes smaller grains (40–60 μm; 20%). Most zircons are light pink to colorless translucent crystals; a few have mineral inclusions. Some zircons have distinct oscillatory zoning. The morphology of the detrital zircons show a wide variety of forms, ranging from subhedral to prismatic euhedral stubby crystals with undamaged faces and corners to strongly rounded zircons with no visible crystalline faces. Grains with well-preserved crystal habit suggest a proximal sedimentary source. Conversely, rounded crystals indicate that the grains have been transported over a long distance or that they have survived more than one cycle of erosion and deposition. Most of the zircons have high Th/U ratios (>0.1) and were probably derived from igneous rocks, whereas a few grains with low ratios (<0.1) may have a metamorphic origin.

The zircon ages obtained (Figs. 5 and 7; Tables 1 and 2) are quite similar in samples WZD-1 and -2. Of the 86 zircon grains from WZD-1 analyzed by SIMS, the majority yielded ages between 760 Ma and 1250 Ma with peak age at ca. 800 Ma. There are also minor age groups of 700–430 Ma, 1800–1700 Ma and 2500–2400 Ma. It is notable that there are three zircon grains in 1500–1300 Ma range, and three Paleoproterozoic detrital zircons form a peak at 2494 Ma. In addition, there are only two Archean zircons with ages of 2850 ± 34 Ma and 2841 ± 35 Ma. The youngest zircon gives an age of 303 ± 4.5 Ma.

For sample WZD-2, 115 grains were analyzed, with 108 spots showing 90–110% concordance. These findings are quite similar

Table 1
U–Pb SIMS ages of detrital zircons from the bauxite ores sample WZD-1 in the WZD area.

Samples spot #	U (ppm)	Th (ppm)	Th/U	$^{206}Pb^{*}$ (ppm)	f_{206} (%)	Isotopic ratio						Age/Ma			
						$^{207}Pb^{*}/^{206}Pb^{*}$	±%	$^{207}Pb^{*}/^{235}U$	±%	$^{206}Pb^{*}/^{238}U$	±%	$^{206}Pb^{*}/^{238}U$	±1σ	$^{207}Pb^{*}/^{206}Pb^{*}$	±1σ
WZD-1-1	93	35	0.37	18	0.10	0.07075	2.37	1.58145	2.81	0.16211	1.50	968	14	950	48
WZD-1-2	90	106	1.18	17	0.13	0.06249	1.81	1.14975	2.35	0.13344	1.50	807	11	691	38
WZD-1-3	54	0	0.00	19	0.12	0.11254	1.09	5.07366	1.85	0.32697	1.50	1824	24	1841	20
WZD-1-4	258	247	0.96	17	0.14	0.05181	2.75	0.34389	3.14	0.04814	1.50	303	4	277	62
WZD-1-5	188	140	0.74	32	0.06	0.06591	1.18	1.19532	1.91	0.13152	1.50	797	11	804	25
WZD-1-6	57	19	0.33	11	0.28	0.07066	2.17	1.56289	2.64	0.16041	1.50	959	13	948	44
WZD-1-7	70	89	1.28	14	0.22	0.06085	2.26	1.12378	2.71	0.13393	1.50	810	11	634	48
WZD-1-8	123	81	0.66	30	0.11	0.07740	1.17	2.03375	1.92	0.19058	1.53	1124	16	1131	23
WZD-1-9	77	43	0.56	15	0.15	0.06820	1.81	1.44395	2.35	0.15356	1.50	921	13	875	37
WZD-1-10	195	142	0.73	72	0.03	0.10138	0.62	3.95340	1.63	0.28282	1.50	1606	21	1650	12
WZD-1-11	165	439	2.67	41	0.03	0.06725	1.16	1.20861	1.91	0.13035	1.51	790	11	845	24
WZD-1-12	66	48	0.72	11	0.10	0.06646	1.89	1.21387	2.42	0.13246	1.50	802	11	821	39
WZD-1-13	182	122	0.67	39	0.02	0.07244	0.92	1.66765	1.77	0.16696	1.52	995	14	998	18
WZD-1-14	130	86	0.66	12	0.10	0.05542	2.11	0.54163	2.61	0.07088	1.54	441	7	429	46
WZD-1-15	159	259	1.63	21	0.04	0.05612	1.57	0.64476	2.17	0.08333	1.50	516	7	457	34
WZD-1-16	172	139	0.81	36	0.07	0.06921	1.03	1.52127	1.82	0.15942	1.50	954	13	905	21
WZD-1-17	270	94	0.35	57	0.05	0.07451	0.77	1.81526	1.69	0.17669	1.50	1049	15	1055	15
WZD-1-18	117	85	0.73	10	0.11	0.05610	2.19	0.53739	2.65	0.06947	1.50	433	6	456	48
WZD-1-19	517	43	0.08	95	0.01	0.07233	0.65	1.67646	1.63	0.16809	1.50	1002	14	995	13
WZD-1-20	100	138	1.37	43	0.02	0.09732	0.83	3.84405	1.73	0.28647	1.52	1624	22	1573	16
WZD-1-21	126	72	0.57	51	0.03	0.10787	0.67	4.73564	1.65	0.31841	1.50	1782	23	1764	12
WZD-1-22	285	137	0.48	53	0.00	0.07089	0.91	1.48246	1.77	0.15168	1.51	910	13	954	19
WZD-1-23	89	35	0.40	18	0.02	0.07476	1.95	1.73042	2.46	0.16788	1.50	1000	14	1062	39
WZD-1-24	76	103	1.36	10	0.00	0.05824	2.21	0.69181	2.68	0.08615	1.51	533	8	539	48
WZD-1-25	450	354	0.79	280	0.01	0.16384	0.25	10.14956	1.52	0.44928	1.50	2392	30	2496	4
WZD-1-26	463	181	0.39	133	0.02	0.09077	0.54	2.99105	1.65	0.23900	1.56	1381	19	1442	10
WZD-1-27	171	114	0.67	36	0.07	0.07127	1.03	1.60337	1.82	0.16317	1.50	974	14	965	21
WZD-1-28	372	239	0.64	147	0.01	0.10601	0.41	4.47228	1.56	0.30596	1.51	1721	23	1732	8
WZD-1-29	77	93	1.21	11	0.00	0.06147	2.07	0.81379	2.57	0.09601	1.53	591	9	656	44
WZD-1-30	245	198	0.81	99	0.02	0.10628	0.52	4.43786	1.59	0.30285	1.50	1705	23	1737	9
WZD-1-31	141	223	1.58	18	0.08	0.05812	1.85	0.66405	2.38	0.08286	1.51	513	7	534	40
WZD-1-32	333	385	1.16	78	0.01	0.07212	0.87	1.63417	1.93	0.16433	1.73	981	16	989	18
WZD-1-33	115	211	1.85	24	0.04	0.06567	1.68	1.15485	2.26	0.12754	1.51	774	11	796	35
WZD-1-34	148	39	0.27	30	0.02	0.07456	1.80	1.80719	2.35	0.17578	1.50	1044	14	1057	36
WZD-1-35	184	173	0.94	38	0.11	0.06940	1.11	1.49340	1.87	0.15607	1.50	935	13	911	23
WZD-1-36	92	147	1.59	12	0.00	0.05909	2.08	0.67527	2.58	0.08289	1.52	513	7	570	45
WZD-1-37	440	116	0.26	132	0.02	0.09002	0.57	3.17330	1.61	0.25566	1.50	1468	20	1426	11
WZD-1-38	297	147	0.50	41	0.87	0.05901	4.42	0.92961	4.68	0.11426	1.55	697	10	567	93
WZD-1-39	387	5	0.01	39	0.03	0.05980	1.13	0.78195	1.89	0.09484	1.51	584	8	596	24
WZD-1-40	143	132	0.93	24	0.10	0.06463	1.37	1.12937	2.04	0.12674	1.50	769	11	762	29
WZD-1-41	150	359	2.40	24	0.14	0.05821	1.79	0.69836	2.33	0.08701	1.50	538	8	538	39
WZD-1-42	142	156	1.10	34	0.04	0.07403	1.07	1.69668	2.16	0.16621	1.88	991	17	1042	22
WZD-1-43	515	241	0.47	134	0.03	0.08212	0.73	2.42613	1.67	0.21427	1.50	1252	17	1248	14
WZD-1-44	141	214	1.52	40	0.13	0.07715	1.25	1.99208	1.95	0.18726	1.50	1107	15	1125	25
WZD-1-45	229	35	0.15	27	0.06	0.06155	1.17	0.91477	1.90	0.10780	1.50	660	9	658	25

WZD-1-46	264	451	1.71	35	0.00	0.05930	1.57	0.67723	2.17	0.08282	1.50	513	7	578	34
WZD-1-47	134	50	0.37	32	0.09	0.07876	1.03	2.20446	2.03	0.20300	1.75	1191	19	1166	20
WZD-1-48	253	169	0.67	23	0.05	0.05566	1.69	0.54817	2.36	0.07143	1.65	445	7	439	37
WZD-1-49	117	37	0.32	23	0.03	0.07108	1.20	1.61639	1.93	0.16494	1.50	984	14	960	24
WZD-1-50	148	114	0.77	25	0.10	0.06564	1.35	1.19647	2.02	0.13220	1.50	800	11	795	28
WZD-1-51	125	186	1.48	25	0.10	0.06516	1.59	1.18302	2.19	0.13168	1.50	797	11	779	33
WZD-1-52	204	179	0.88	116	0.11	0.16391	0.69	9.51426	1.65	0.42100	1.50	2265	29	2496	12
WZD-1-53	251	102	0.41	139	0.01	0.16388	0.37	9.82695	1.83	0.43490	1.80	2328	35	2496	6
WZD-1-54	27	28	1.05	22	0.28	0.21750	0.95	16.67000	1.79	0.55588	1.52	2850	35	2962	15
WZD-1-55	476	258	0.54	54	0.01	0.05871	0.96	0.74444	1.78	0.09196	1.50	567	8	556	21
WZD-1-56	67	59	0.88	11	0.18	0.06182	2.39	1.06449	2.83	0.12489	1.50	759	11	668	50
WZD-1-57	172	105	0.61	130	0.04	0.20090	0.38	15.34006	1.55	0.55380	1.50	2841	35	2833	6
WZD-1-58	441	361	0.82	128	0.21	0.08823	0.59	2.68626	1.62	0.22083	1.51	1286	18	1387	11
WZD-1-59	400	295	0.74	82	0.15	0.07137	0.87	1.59661	1.74	0.16225	1.51	969	14	968	18
WZD-1-60	579	108	0.19	100	0.21	0.07015	0.65	1.49046	1.63	0.15409	1.50	924	13	933	13
WZD-1-61	197	207	1.05	55	4.59	0.08549	2.77	2.32207	3.15	0.19701	1.51	1159	16	1327	53
WZD-1-62	268	461	1.72	57	0.05	0.06542	1.17	1.19734	1.90	0.13274	1.50	803	11	788	24
WZD-1-63	240	156	0.65	95	0.01	0.10679	0.54	4.48404	1.60	0.30453	1.50	1714	23	1745	10
WZD-1-64	892	1316	1.48	197	2.09	0.07482	1.09	1.59302	1.85	0.15442	1.50	926	13	1064	22
WZD-1-65	234	108	0.46	50	0.07	0.07360	0.91	1.79060	1.75	0.17645	1.50	1048	15	1031	18
WZD-1-66	188	132	0.70	49	0.03	0.08317	1.13	2.27913	1.95	0.19874	1.60	1169	17	1273	22
WZD-1-67	485	182	0.38	107	0.02	0.07561	0.53	1.92630	1.59	0.18478	1.50	1093	15	1085	11
WZD-1-68	847	71	0.08	264	0.02	0.10932	0.40	4.14780	1.55	0.27517	1.50	1567	21	1788	7
WZD-1-69	248	89	0.36	44	0.22	0.06933	1.02	1.44171	1.82	0.15082	1.51	906	13	909	21
WZD-1-70	140	165	1.18	26	0.16	0.06406	1.87	1.16398	2.43	0.13179	1.56	798	12	744	39
WZD-1-71	289	164	0.57	78	0.22	0.08208	0.74	2.41985	1.68	0.21383	1.51	1249	17	1247	14
WZD-1-72	222	193	0.87	39	0.11	0.06483	1.40	1.19601	2.06	0.13380	1.52	810	12	769	29
WZD-1-73	101	93	0.92	18	0.36	0.06486	1.82	1.20884	2.36	0.13517	1.50	817	12	770	38
WZD-1-74	266	194	0.73	36	0.02	0.06137	1.02	0.89687	1.82	0.10599	1.50	649	9	652	22
WZD-1-75	653	450	0.69	137	0.01	0.07132	0.58	1.60940	1.61	0.16366	1.50	977	14	967	12
WZD-1-76	151	597	3.94	32	0.05	0.06077	1.55	0.79328	2.16	0.09467	1.50	583	8	631	33
WZD-1-77	135	109	0.81	33	0.04	0.07728	1.39	1.95808	2.08	0.18376	1.55	1087	15	1128	28
WZD-1-78	212	100	0.47	40	0.02	0.06964	0.90	1.47360	1.75	0.15346	1.50	920	13	918	18
WZD-1-79	64	96	1.49	19	0.03	0.07721	1.41	2.09291	2.06	0.19660	1.50	1157	16	1127	28
WZD-1-80	133	69	0.52	26	0.10	0.07042	1.34	1.56045	2.01	0.16071	1.50	961	13	941	27
WZD-1-81	274	347	1.27	37	0.11	0.05775	1.62	0.73500	2.21	0.09231	1.50	569	8	520	35
WZD-1-82	212	135	0.64	36	0.81	0.06534	5.21	1.22696	5.43	0.13618	1.52	823	12	785	106
WZD-1-83	74	51	0.69	14	0.06	0.06809	1.94	1.36517	2.46	0.14541	1.50	875	12	871	40
WZD-1-84	202	155	0.77	35	0.05	0.06697	1.31	1.23865	1.99	0.13415	1.50	812	11	837	27
WZD-1-85	299	34	0.11	31	0.02	0.05971	1.11	0.78357	1.87	0.09517	1.51	586	8	593	24
WZD-1-86	250	122	0.49	56	0.04	0.07444	0.80	1.88208	1.71	0.18337	1.51	1085	15	1053	16

Errors are 1σ; f_{206} is the percentage of common ^{206}Pb in total ^{206}Pb; Common Pb corrected using the measured ^{204}Pb.

Table 2
U–Pb LA-ICP-MS ages of detrital zircons from the bauxite ores sample (WZD-2) and mud shale of the Hanjiadian Group samples (WZD-3 and WZD-4) in the WZD area in western Yangtze Block, SW China.

Samples spot #	U (ppm)	Th (ppm)	Th/U	Isotopic ratio						Age/Ma						Conc. (%)
				$^{207}Pb/^{206}Pb$	±1σ	$^{207}Pb/^{235}U$	±1σ	$^{206}Pb/^{238}U$	±1σ	$^{206}Pb/^{238}U$	±1σ	$^{207}Pb/^{206}Pb$	±1σ	$^{207}Pb/^{235}U$	±1σ	
Sample WZD-2 (bauxite ores), 115 grains measured, 108 are concordant in the range of 90–110%, only concordant grains are shown																
WZD-2-1	558	140	0.25	0.0699	0.0021	1.4528	0.0206	0.1508	0.0021	906	11	925	13	911	9	101
WZD-2-2	148	56	0.38	0.0725	0.0023	1.6728	0.0293	0.1675	0.0024	998	13	999	16	998	11	100
WZD-2-3	324	227	0.70	0.0558	0.0018	0.5434	0.0103	0.0707	0.0010	440	6	443	20	441	7	100
WZD-2-4	374	143	0.38	0.1549	0.0045	8.5256	0.1160	0.3994	0.0054	2166	25	2401	11	2289	12	110
WZD-2-5	268	145	0.54	0.1126	0.0033	5.1011	0.0703	0.3287	0.0045	1832	22	1842	11	1836	12	101
WZD-2-7	188	178	0.95	0.0691	0.0021	1.4154	0.0230	0.1486	0.0021	893	12	902	15	895	10	100
WZD-2-8	320	88	0.27	0.0672	0.0020	1.2733	0.0189	0.1375	0.0019	831	11	843	14	834	8	100
WZD-2-9	84	16	0.19	0.0738	0.0024	1.6389	0.0313	0.1611	0.0023	963	13	1036	18	985	12	108
WZD-2-10	776	399	0.51	0.0675	0.0020	1.3121	0.0184	0.1410	0.0019	850	11	853	13	851	8	100
WZD-2-11	103	30	0.29	0.0715	0.0024	1.5850	0.0311	0.1609	0.0023	961	13	971	19	964	12	100
WZD-2-12	339	286	0.84	0.0752	0.0023	1.8384	0.0265	0.1774	0.0024	1053	13	1073	13	1059	9	102
WZD-2-13	287	141	0.49	0.0705	0.0022	1.3914	0.0213	0.1431	0.0020	862	11	944	14	885	9	103
WZD-2-15	517	307	0.59	0.0772	0.0024	1.6009	0.0242	0.1504	0.0021	903	11	1127	13	971	9	108
WZD-2-16	189	93	0.49	0.0600	0.0021	0.8298	0.0265	0.1004	0.0014	616	8	603	78	614	15	100
WZD-2-17	235	83	0.35	0.0745	0.0023	1.8013	0.0274	0.1754	0.0024	1042	13	1055	14	1046	10	101
WZD-2-18	235	116	0.49	0.1579	0.0047	9.9564	0.1370	0.4575	0.0062	2429	27	2433	11	2431	13	100
WZD-2-19	175	110	0.63	0.0688	0.0022	1.3915	0.0242	0.1468	0.0020	883	11	891	17	885	10	100
WZD-2-20	450	379	0.84	0.1436	0.0040	7.6061	0.1802	0.3841	0.0057	2095	27	2271	49	2186	21	108
WZD-2-21	246	159	0.64	0.0652	0.0021	1.0645	0.0186	0.1184	0.0016	721	9	781	17	736	9	102
WZD-2-22	582	88	0.15	0.0669	0.0015	1.2118	0.0215	0.1313	0.0018	795	10	836	47	806	10	101
WZD-2-23	339	174	0.51	0.0755	0.0023	1.8639	0.0260	0.1790	0.0024	1061	13	1082	13	1068	9	102
WZD-2-24	777	401	0.52	0.2901	0.0087	27.8345	0.3784	0.6957	0.0094	3404	36	3418	10	3413	13	100
WZD-2-25	165	101	0.61	0.0616	0.0019	0.8956	0.0144	0.1054	0.0015	646	8	662	15	649	8	100
WZD-2-26	226	184	0.81	0.0918	0.0028	3.1314	0.0437	0.2474	0.0034	1425	17	1463	12	1440	11	103
WZD-2-27	144	119	0.82	0.0807	0.0025	2.2041	0.0338	0.1980	0.0027	1164	15	1215	13	1182	11	104
WZD-2-28	655	334	0.51	0.0754	0.0023	1.8898	0.0260	0.1818	0.0025	1077	13	1078	13	1077	9	100
WZD-2-29	109	57	0.52	0.1845	0.0056	13.1890	0.1819	0.5184	0.0071	2692	30	2694	10	2693	13	100
WZD-2-30	183	142	0.77	0.0790	0.0024	2.1709	0.0311	0.1993	0.0027	1171	15	1172	13	1172	10	100
WZD-2-31	181	168	0.93	0.0739	0.0023	1.7045	0.0260	0.1672	0.0023	996	13	1040	14	1010	10	104
WZD-2-32	281	169	0.60	0.1149	0.0035	5.3495	0.0739	0.3375	0.0046	1875	22	1879	11	1877	12	100
WZD-2-33	27	35	1.27	0.0671	0.0025	1.2260	0.0313	0.1325	0.0020	802	11	841	29	813	14	101
WZD-2-34	119	57	0.48	0.0693	0.0022	1.3975	0.0224	0.1463	0.0020	880	11	906	15	888	9	101
WZD-2-35	118	144	1.22	0.0820	0.0061	2.3038	0.1674	0.2039	0.0036	1196	19	1245	151	1213	51	104
WZD-2-37	162	160	0.99	0.0714	0.0022	1.5073	0.0218	0.1531	0.0021	918	12	969	13	933	9	102
WZD-2-39	202	174	0.86	0.0892	0.0027	2.9726	0.0414	0.2416	0.0033	1395	17	1409	12	1401	11	101
WZD-2-40	321	229	0.71	0.0596	0.0018	0.8068	0.0117	0.0983	0.0013	604	8	587	14	601	7	100
WZD-2-41	417	226	0.54	0.1590	0.0048	10.1011	0.1369	0.4607	0.0062	2443	28	2445	10	2444	13	100
WZD-2-42	382	361	0.95	0.1613	0.0048	9.8762	0.1344	0.4439	0.0060	2368	27	2470	11	2423	13	104
WZD-2-43	332	177	0.53	0.0681	0.0021	1.5104	0.0212	0.1608	0.0022	961	12	872	13	935	9	97
WZD-2-44	228	205	0.90	0.1585	0.0048	8.9355	0.1222	0.4088	0.0056	2209	25	2440	11	2331	12	110
WZD-2-45	31	9	0.30	0.0702	0.0023	1.5517	0.0302	0.1604	0.0023	959	13	933	19	951	12	99
WZD-2-46	834	262	0.31	0.0571	0.0017	0.7213	0.0101	0.0917	0.0013	565	7	494	14	551	6	98
WZD-2-47	141	313	2.23	0.0717	0.0022	1.1899	0.0185	0.1203	0.0017	732	9	979	14	796	9	109
WZD-2-48	430	299	0.70	0.0705	0.0021	1.5278	0.0212	0.1572	0.0021	941	12	943	13	942	9	100
WZD-2-49	191	125	0.65	0.0738	0.0022	1.7735	0.0259	0.1742	0.0024	1035	13	1037	13	1036	9	100
WZD-2-50	182	99	0.55	0.1599	0.0048	10.1996	0.1394	0.4626	0.0063	2451	28	2454	11	2453	13	100
WZD-2-51	47	19	0.40	0.0701	0.0022	1.4956	0.0262	0.1548	0.0022	928	12	931	17	929	11	100
WZD-2-52	102	71	0.70	0.0663	0.0021	1.2311	0.0198	0.1347	0.0019	815	11	815	15	815	9	100
WZD-2-53	923	517	0.56	0.1593	0.0047	9.0513	0.1223	0.4122	0.0056	2225	26	2448	10	2343	12	110
WZD-2-54	98	257	2.61	0.0581	0.0019	0.6841	0.0122	0.0854	0.0012	528	7	532	18	529	7	100
WZD-2-55	159	71	0.44	0.1069	0.0032	4.5839	0.0637	0.3111	0.0042	1746	21	1747	12	1746	12	100
WZD-2-56	355	188	0.53	0.1708	0.0051	11.2841	0.1538	0.4792	0.0065	2524	28	2565	10	2547	13	102

WZD-2-57	167	291	1.74	0.0815	0.0025	2.3712	0.0339	0.2110	0.0029	1234	15	1234	13	1234	10	100
WZD-2-58	219	191	0.87	0.0729	0.0022	1.6983	0.0242	0.1690	0.0023	1007	13	1010	13	1008	9	100
WZD-2-59	69	62	0.89	0.1170	0.0036	5.5372	0.0830	0.3434	0.0049	1903	24	1910	12	1906	13	100
WZD-2-60	278	195	0.70	0.0759	0.0023	1.9291	0.0288	0.1844	0.0026	1091	14	1092	13	1091	10	100
WZD-2-61	242	111	0.46	0.0741	0.0022	1.7201	0.0433	0.1683	0.0025	1003	14	1045	60	1016	16	104
WZD-2-62	159	171	1.08	0.1638	0.0050	10.6744	0.1556	0.4726	0.0067	2495	29	2495	11	2495	14	100
WZD-2-63	150	307	2.05	0.0616	0.0020	0.7520	0.0127	0.0886	0.0013	547	8	659	16	569	7	104
WZD-2-64	293	177	0.60	0.0639	0.0020	0.9415	0.0144	0.1068	0.0015	654	9	739	14	674	8	103
WZD-2-65	519	1323	2.55	0.0707	0.0022	1.5230	0.0222	0.1563	0.0022	936	12	948	13	940	9	100
WZD-2-66	237	129	0.54	0.1137	0.0035	4.7978	0.0696	0.3059	0.0043	1721	21	1860	12	1785	12	108
WZD-2-67	203	228	1.12	0.1586	0.0048	9.9227	0.1431	0.4537	0.0064	2412	29	2441	11	2428	13	101
WZD-2-68	207	280	1.35	0.0992	0.0030	3.8528	0.0564	0.2817	0.0040	1600	20	1609	12	1604	12	101
WZD-2-69	329	182	0.55	0.0805	0.0024	2.3148	0.0602	0.2087	0.0031	1222	16	1208	60	1217	18	99
WZD-2-70	178	140	0.79	0.0997	0.0030	3.7290	0.0539	0.2712	0.0038	1547	19	1619	12	1578	12	105
WZD-2-71	509	399	0.78	0.0602	0.0018	0.6150	0.0091	0.0740	0.0011	460	6	612	14	487	6	106
WZD-2-72	341	252	0.74	0.0728	0.0022	1.6368	0.0241	0.1631	0.0023	974	13	1008	13	984	9	103
WZD-2-73	747	183	0.24	0.0604	0.0018	0.8199	0.0118	0.0984	0.0014	605	8	619	14	608	7	100
WZD-2-74	669	96	0.14	0.0741	0.0022	1.7775	0.0254	0.1741	0.0025	1034	13	1043	13	1037	9	101
WZD-2-75	127	151	1.19	0.0682	0.0021	0.9741	0.0156	0.1036	0.0015	635	9	874	15	691	8	109
WZD-2-76	329	230	0.70	0.0754	0.0023	1.8846	0.0272	0.1811	0.0026	1073	14	1080	13	1076	10	101
WZD-2-77	106	78	0.74	0.1101	0.0033	4.8673	0.0706	0.3205	0.0045	1792	22	1801	12	1797	12	101
WZD-2-78	245	218	0.89	0.0759	0.0023	1.9213	0.0277	0.1835	0.0026	1086	14	1093	13	1089	10	101
WZD-2-79	344	214	0.62	0.0774	0.0023	1.8785	0.0271	0.1760	0.0025	1045	14	1132	13	1074	10	108
WZD-2-80	440	410	0.93	0.0629	0.0019	0.7588	0.0111	0.0875	0.0012	541	7	705	14	573	6	106
WZD-2-81	451	373	0.83	0.0920	0.0028	3.2163	0.0454	0.2536	0.0036	1457	18	1466	12	1461	11	101
WZD-2-82	322	127	0.39	0.0738	0.0022	1.7158	0.0246	0.1685	0.0024	1004	13	1037	13	1014	9	103
WZD-2-83	293	204	0.69	0.0571	0.0017	0.5621	0.0085	0.0714	0.0010	444	6	496	15	453	6	102
WZD-2-84	61	78	1.27	0.0779	0.0024	1.8476	0.0296	0.1719	0.0025	1022	13	1145	14	1063	11	110
WZD-2-85	322	241	0.75	0.0717	0.0022	1.6085	0.0230	0.1626	0.0023	971	13	978	13	974	9	100
WZD-2-86	186	95	0.51	0.0605	0.0018	1.1694	0.0176	0.1402	0.0020	846	11	620	14	786	8	93
WZD-2-87	146	155	1.07	0.0678	0.0021	1.2429	0.0193	0.1328	0.0019	804	11	864	14	820	9	102
WZD-2-88	913	121	0.13	0.0713	0.0008	1.5824	0.0105	0.1610	0.0008	962	4	965	7	963	4	100
WZD-2-89	213	103	0.48	0.0646	0.0011	1.1155	0.0154	0.1251	0.0007	760	4	762	19	761	7	100
WZD-2-90	88	28	0.32	0.0758	0.0015	1.8708	0.0332	0.1790	0.0013	1062	7	1088	24	1071	12	102
WZD-2-91	62	24	0.38	0.1698	0.0022	11.3494	0.1061	0.4846	0.0032	2547	14	2556	8	2552	9	100
WZD-2-92	265	72	0.27	0.0719	0.0010	1.5968	0.0173	0.1610	0.0009	962	5	983	13	969	7	101
WZD-2-93	1005	1178	1.17	0.0770	0.0009	1.6115	0.0113	0.1518	0.0007	911	4	1121	7	975	4	107
WZD-2-94	224	142	0.63	0.0731	0.0010	1.6860	0.0175	0.1672	0.0009	996	5	1018	12	1003	7	102
WZD-2-95	256	245	0.96	0.0593	0.0011	0.7155	0.0108	0.0875	0.0005	541	3	578	22	548	6	101
WZD-2-96	483	267	0.55	0.1525	0.0022	8.4120	0.0933	0.4001	0.0028	2169	13	2374	10	2276	10	109
WZD-2-97	101	146	1.45	0.0677	0.0017	1.2584	0.0297	0.1347	0.0011	815	6	860	35	827	13	101
WZD-2-98	279	141	0.50	0.0763	0.0011	1.9504	0.0207	0.1855	0.0010	1097	6	1102	13	1099	7	100
WZD-2-101	235	156	0.66	0.1050	0.0013	4.4005	0.0364	0.3040	0.0016	1711	8	1714	8	1712	7	100
WZD-2-102	24	5	0.21	0.1761	0.0036	12.0265	0.2245	0.4953	0.0056	2594	24	2616	17	2606	18	101
WZD-2-104	141	125	0.89	0.1521	0.0021	9.2307	0.1104	0.4401	0.0028	2351	12	2370	24	2361	11	101
WZD-2-105	227	118	0.52	0.1148	0.0013	5.3356	0.0388	0.3372	0.0018	1873	8	1876	6	1875	6	100
WZD-2-106	121	50	0.42	0.0750	0.0015	1.7656	0.0316	0.1709	0.0012	1017	7	1067	24	1033	12	105
WZD-2-107	421	920	2.18	0.0619	0.0013	0.7971	0.0150	0.0935	0.0006	576	4	669	29	595	8	103
WZD-2-108	205	112	0.55	0.0738	0.0011	1.7158	0.0197	0.1687	0.0010	1005	5	1035	14	1014	7	103
WZD-2-109	497	590	1.19	0.1061	0.0013	4.0373	0.0344	0.2759	0.0015	1571	8	1734	8	1642	7	110
WZD-2-110	263	110	0.42	0.0713	0.0012	1.5444	0.0219	0.1571	0.0010	941	5	966	19	948	9	101
WZD-2-111	237	146	0.61	0.0677	0.0011	1.2867	0.0178	0.1379	0.0008	833	5	858	19	840	8	101
WZD-2-112	364	168	0.46	0.0725	0.0010	1.6781	0.0158	0.1678	0.0009	1000	5	1001	11	1000	6	100
WZD-2-113	645	545	0.84	0.0982	0.0011	3.7604	0.0250	0.2778	0.0014	1580	7	1590	6	1584	5	101
WZD-2-114	210	75	0.36	0.0812	0.0012	2.2489	0.0256	0.2009	0.0012	1180	6	1226	13	1196	8	104
WZD-2-115	293	291	0.99	0.0712	0.0021	1.5390	0.0223	0.1569	0.0021	939	12	963	13	946	9	101
Sample WZD-3 (mud shale of the Hanjiadian Group), 91 grains measured, 86 are concordant in the range of 90–110%, only concordant grains are shown																
WZD-3-1	75	33	0.44	0.0691	0.0022	1.1036	0.0202	0.1159	0.0017	707	10	901	17	755	10	107

(*continued on next page*)

Table 2 (*continued*)

Samples spot #	U (ppm)	Th (ppm)	Th/U	Isotopic ratio						Age/Ma						Conc. (%)
				$^{207}Pb/^{206}Pb$	±1σ	$^{207}Pb/^{235}U$	±1σ	$^{206}Pb/^{238}U$	±1σ	$^{206}Pb/^{238}U$	±1σ	$^{207}Pb/^{206}Pb$	±1σ	$^{207}Pb/^{235}U$	±1σ	
WZD-3-2	185	117	0.63	0.0741	0.0022	1.7924	0.0263	0.1755	0.0025	1042	14	1043	13	1043	10	100
WZD-3-3	536	141	0.26	0.1644	0.0049	10.3989	0.1472	0.4588	0.0065	2434	29	2501	11	2471	13	103
WZD-3-4	475	152	0.32	0.0633	0.0020	1.0259	0.0159	0.1175	0.0017	716	10	720	15	717	8	100
WZD-3-5	861	1163	1.35	0.1647	0.0050	10.2642	0.1467	0.4520	0.0064	2404	28	2504	11	2459	13	104
WZD-3-6	205	166	0.81	0.0699	0.0021	1.4744	0.0220	0.1531	0.0022	918	12	924	14	920	9	100
WZD-3-7	105	130	1.24	0.0591	0.0019	0.7441	0.0137	0.0913	0.0013	563	8	570	18	565	8	100
WZD-3-8	146	140	0.95	0.0783	0.0024	1.9794	0.0310	0.1834	0.0026	1086	14	1153	14	1109	11	106
WZD-3-9	115	99	0.86	0.0688	0.0022	1.2634	0.0205	0.1331	0.0019	805	11	894	15	829	9	103
WZD-3-10	322	400	1.24	0.0748	0.0023	1.6377	0.0244	0.1587	0.0023	950	13	1064	13	985	9	104
WZD-3-11	344	256	0.74	0.1626	0.0050	10.1219	0.1485	0.4515	0.0065	2402	29	2483	11	2446	14	103
WZD-3-12	305	164	0.54	0.0748	0.0023	1.8474	0.0277	0.1791	0.0026	1062	14	1064	14	1063	10	100
WZD-3-13	655	367	0.56	0.0769	0.0024	1.4166	0.0213	0.1337	0.0019	809	11	1118	13	896	9	138
WZD-3-14	88	101	1.15	0.1170	0.0037	4.9723	0.0774	0.3081	0.0045	1731	22	1912	12	1815	13	110
WZD-3-15	384	282	0.74	0.0800	0.0025	2.2446	0.0336	0.2035	0.0029	1194	16	1197	13	1195	11	100
WZD-3-16	302	316	1.05	0.1607	0.0049	9.6935	0.1425	0.4375	0.0063	2339	28	2463	11	2406	14	105
WZD-3-17	212	112	0.53	0.1731	0.0053	11.4951	0.1694	0.4817	0.0069	2535	30	2587	11	2564	14	102
WZD-3-18	428	70	0.16	0.1868	0.0039	13.0357	0.1986	0.5061	0.0072	2640	31	2714	35	2682	14	103
WZD-3-19	274	231	0.84	0.1642	0.0050	10.8396	0.1590	0.4787	0.0069	2522	30	2500	11	2509	14	99
WZD-3-20	239	127	0.53	0.1056	0.0029	4.3804	0.1007	0.3008	0.0045	1695	22	1725	52	1709	19	102
WZD-3-21	113	57	0.51	0.2524	0.0077	22.3507	0.3257	0.6422	0.0092	3198	36	3200	10	3199	14	100
WZD-3-22	223	287	1.29	0.0733	0.0023	1.6789	0.0251	0.1661	0.0024	990	13	1023	14	1001	10	103
WZD-3-23	82	95	1.16	0.0695	0.0035	1.4654	0.0707	0.1529	0.0025	917	14	914	108	916	29	100
WZD-3-24	268	164	0.61	0.0611	0.0024	0.8322	0.0302	0.0988	0.0015	607	9	643	87	615	17	101
WZD-3-25	411	244	0.59	0.0702	0.0021	1.3335	0.0198	0.1379	0.0020	832	11	933	14	860	9	103
WZD-3-26	651	199	0.31	0.0631	0.0019	0.8531	0.0126	0.0980	0.0014	603	8	713	14	626	7	103
WZD-3-28	385	218	0.57	0.1616	0.0049	10.3848	0.1501	0.4660	0.0066	2466	29	2472	11	2470	13	100
WZD-3-29	314	94	0.30	0.1009	0.0031	3.7209	0.0545	0.2674	0.0038	1527	19	1641	12	1576	12	107
WZD-3-30	99	151	1.53	0.0692	0.0022	1.3376	0.0211	0.1401	0.0020	845	11	906	15	862	9	102
WZD-3-31	200	73	0.36	0.1031	0.0031	4.2339	0.0618	0.2976	0.0042	1680	21	1681	12	1681	12	100
WZD-3-32	135	198	1.46	0.1580	0.0049	9.7358	0.1516	0.4469	0.0065	2382	29	2434	12	2410	14	102
WZD-3-33	175	78	0.45	0.0725	0.0022	1.6633	0.0253	0.1664	0.0024	992	13	999	14	995	10	100
WZD-3-34	167	65	0.39	0.0733	0.0021	1.7866	0.0432	0.1768	0.0026	1049	14	1022	59	1041	16	97
WZD-3-35	175	150	0.86	0.0671	0.0021	1.2770	0.0192	0.1380	0.0020	834	11	840	14	836	9	100
WZD-3-36	197	106	0.54	0.2585	0.0079	23.2310	0.3391	0.6517	0.0093	3235	36	3238	10	3237	14	100
WZD-3-37	192	176	0.91	0.0725	0.0022	1.6410	0.0247	0.1642	0.0023	980	13	999	14	986	10	101
WZD-3-38	247	156	0.63	0.2875	0.0088	27.5483	0.4016	0.6949	0.0099	3401	38	3404	10	3403	14	100
WZD-3-39	463	699	1.51	0.0589	0.0018	0.7031	0.0109	0.0866	0.0012	536	7	562	15	541	6	101
WZD-3-41	51	34	0.66	0.1743	0.0054	11.9269	0.1775	0.4962	0.0071	2598	31	2599	11	2599	14	100
WZD-3-42	460	236	0.51	0.0714	0.0022	1.5660	0.0234	0.1590	0.0023	951	13	970	14	957	9	101
WZD-3-43	374	318	0.85	0.0598	0.0019	0.7301	0.0114	0.0885	0.0013	547	7	596	15	557	7	102
WZD-3-44	114	70	0.62	0.0721	0.0023	1.6237	0.0256	0.1634	0.0023	975	13	988	14	979	10	100
WZD-3-45	424	215	0.51	0.0908	0.0028	3.1358	0.0461	0.2505	0.0036	1441	18	1442	13	1442	11	100
WZD-3-46	661	747	1.13	0.0612	0.0019	0.8849	0.0133	0.1049	0.0015	643	9	645	15	644	7	100
WZD-3-47	306	216	0.70	0.0737	0.0023	1.7223	0.0257	0.1695	0.0024	1010	13	1032	14	1017	10	102
WZD-3-48	153	5	0.03	0.0598	0.0014	0.7734	0.0142	0.0938	0.0013	578	8	597	51	582	8	101
WZD-3-49	283	110	0.39	0.0768	0.0024	1.9874	0.0296	0.1876	0.0027	1108	14	1116	13	1111	10	101
WZD-3-50	198	253	1.28	0.0685	0.0021	1.3692	0.0209	0.1449	0.0021	872	12	885	14	876	9	100
WZD-3-52	108	101	0.93	0.0938	0.0029	3.1545	0.0492	0.2438	0.0035	1406	18	1504	13	1446	12	107
WZD-3-53	318	83	0.26	0.0744	0.0023	1.7810	0.0273	0.1735	0.0025	1032	14	1053	14	1039	10	102
WZD-3-54	425	60	0.14	0.0725	0.0023	1.5748	0.0236	0.1576	0.0022	944	12	999	14	960	9	102
WZD-3-55	472	449	0.95	0.0668	0.0021	1.2392	0.0190	0.1344	0.0018	813	10	833	14	819	9	101
WZD-3-56	131	74	0.57	0.1880	0.0058	13.5881	0.1929	0.5243	0.0071	2717	30	2724	11	2721	13	100
WZD-3-57	934	623	0.67	0.1352	0.0042	7.0805	0.1003	0.3799	0.0052	2076	24	2166	11	2122	13	104
WZD-3-58	207	147	0.71	0.0694	0.0016	1.1808	0.0209	0.1235	0.0017	750	10	910	47	792	10	106

WZD-3-59	139	57	0.41	0.0650	0.0022	1.0161	0.0192	0.1133	0.0016	692	9	775	19	712	10	103
WZD-3-60	884	1375	1.56	0.0996	0.0032	2.9665	0.0512	0.2160	0.0030	1261	16	1616	15	1399	13	108
WZD-3-61	462	258	0.56	0.0728	0.0023	1.6740	0.0248	0.1668	0.0023	994	12	1008	13	999	9	101
WZD-3-62	153	72	0.47	0.0749	0.0024	1.7975	0.0305	0.1741	0.0024	1035	13	1065	16	1045	11	103
WZD-3-63	841	122	0.14	0.0981	0.0031	3.7650	0.0579	0.2782	0.0038	1582	19	1589	13	1585	12	100
WZD-3-65	349	132	0.38	0.0630	0.0020	0.9239	0.0157	0.1063	0.0015	651	9	709	16	664	8	102
WZD-3-66	354	166	0.47	0.1654	0.0051	10.8288	0.1521	0.4748	0.0065	2505	28	2512	11	2509	13	100
WZD-3-67	128	108	0.84	0.0806	0.0026	2.2286	0.0380	0.2004	0.0028	1178	15	1212	15	1190	12	103
WZD-3-68	700	490	0.70	0.0807	0.0025	1.9545	0.0285	0.1757	0.0024	1044	13	1213	13	1100	10	106
WZD-3-69	80	33	0.41	0.0734	0.0020	1.5264	0.0346	0.1509	0.0022	906	12	1024	55	941	14	104
WZD-3-70	51	26	0.52	0.0798	0.0022	2.0530	0.0486	0.1865	0.0027	1103	15	1193	56	1133	16	108
WZD-3-71	71	116	1.64	0.0771	0.0023	1.9496	0.0511	0.1834	0.0028	1086	15	1124	62	1098	18	103
WZD-3-72	471	140	0.36	0.0758	0.0024	1.9115	0.0281	0.1830	0.0025	1083	14	1089	13	1085	10	101
WZD-3-73	154	132	0.86	0.0732	0.0018	1.3385	0.0275	0.1327	0.0019	803	11	1018	52	863	12	107
WZD-3-74	43	25	0.57	0.1739	0.0055	11.8692	0.1892	0.4950	0.0071	2592	31	2595	12	2594	15	100
WZD-3-75	167	90	0.54	0.0788	0.0018	1.6814	0.0316	0.1548	0.0021	928	12	1167	47	1002	12	108
WZD-3-76	272	156	0.57	0.0595	0.0014	0.5747	0.0112	0.0701	0.0010	437	6	585	53	461	7	105
WZD-3-77	180	258	1.43	0.0681	0.0022	1.2808	0.0230	0.1364	0.0019	824	11	871	17	837	10	102
WZD-3-78	60	82	1.37	0.1770	0.0056	10.8440	0.1689	0.4443	0.0063	2370	28	2625	12	2510	14	110
WZD-3-79	201	92	0.46	0.1169	0.0037	5.5358	0.0822	0.3433	0.0048	1903	23	1910	12	1906	13	100
WZD-3-80	70	27	0.39	0.0774	0.0024	1.7972	0.0497	0.1685	0.0026	1004	14	1131	64	1044	18	104
WZD-3-81	349	146	0.42	0.0731	0.0023	1.7139	0.0275	0.1701	0.0024	1013	13	1016	15	1014	10	100
WZD-3-82	171	78	0.46	0.1461	0.0046	8.6371	0.1273	0.4286	0.0060	2299	27	2301	11	2300	13	100
WZD-3-84	205	21	0.10	0.0700	0.0018	1.4901	0.0312	0.1544	0.0022	926	12	928	53	926	13	100
WZD-3-85	140	92	0.66	0.0710	0.0018	1.3589	0.0282	0.1388	0.0020	838	11	958	53	871	12	104
WZD-3-86	273	362	1.32	0.0754	0.0024	1.7852	0.0291	0.1717	0.0024	1022	13	1079	15	1040	11	106
WZD-3-87	579	348	0.60	0.0751	0.0024	1.8129	0.0283	0.1751	0.0024	1040	13	1071	14	1050	10	103
WZD-3-88	267	68	0.26	0.0754	0.0017	1.5435	0.0275	0.1486	0.0021	893	12	1078	46	948	11	106
WZD-3-89	441	326	0.74	0.0785	0.0025	1.8438	0.0291	0.1704	0.0024	1014	13	1159	14	1061	10	105
WZD-3-90	555	160	0.29	0.0714	0.0016	1.4749	0.0249	0.1499	0.0021	900	12	968	45	920	10	102
WZD-3-91	198	152	0.76	0.0772	0.0025	1.8475	0.0306	0.1736	0.0025	1032	13	1125	15	1063	11	109
Sample WZD-4 (mud shale of the Hanjiadian Group), 45 grains measured, 43 are concordant in the range of 90–110%, only concordant grains are shown																
WZD-4-1	142	247	1.74	0.0582	0.0019	0.6919	0.0114	0.0862	0.0012	533	7	537	16	534	7	100
WZD-4-2	281	194	0.69	0.0746	0.0023	1.3716	0.0214	0.1333	0.0019	807	11	1058	14	877	9	109
WZD-4-3	95	118	1.25	0.0657	0.0021	1.1595	0.0191	0.1279	0.0018	776	10	797	15	782	9	101
WZD-4-4	253	117	0.46	0.0681	0.0021	1.3509	0.0206	0.1438	0.0021	866	12	872	14	868	9	100
WZD-4-5	76	58	0.76	0.0687	0.0022	1.3062	0.0225	0.1380	0.0020	833	11	888	16	848	10	102
WZD-4-6	327	215	0.66	0.0864	0.0027	2.6947	0.0400	0.2263	0.0032	1315	17	1346	13	1327	11	102
WZD-4-7	156	78	0.50	0.0789	0.0025	2.1446	0.0326	0.1971	0.0028	1160	15	1169	13	1163	11	101
WZD-4-8	129	210	1.63	0.1648	0.0051	10.6710	0.1572	0.4694	0.0067	2481	29	2506	11	2495	14	101
WZD-4-9	280	279	1.00	0.0782	0.0024	2.0492	0.0308	0.1900	0.0027	1121	15	1152	13	1132	10	103
WZD-4-10	52	57	1.10	0.0692	0.0024	1.2441	0.0263	0.1304	0.0019	790	11	904	21	821	12	104
WZD-4-12	104	110	1.05	0.0702	0.0023	1.3202	0.0227	0.1363	0.0020	824	11	935	16	855	10	104
WZD-4-13	99	31	0.31	0.0603	0.0019	0.8266	0.0225	0.0995	0.0015	611	9	614	68	612	12	100
WZD-4-14	124	165	1.33	0.0604	0.0020	0.7753	0.0135	0.0931	0.0013	574	8	617	17	583	8	102
WZD-4-15	509	399	0.78	0.1587	0.0049	9.6857	0.1433	0.4425	0.0063	2362	28	2442	11	2405	14	103
WZD-4-16	102	77	0.75	0.0696	0.0029	1.3019	0.0511	0.1357	0.0021	820	12	916	89	847	23	103
WZD-4-17	77	68	0.89	0.1565	0.0049	9.6167	0.1483	0.4457	0.0064	2376	29	2418	12	2399	14	102
WZD-4-18	202	130	0.65	0.0693	0.0025	1.4119	0.0452	0.1477	0.0022	888	13	908	75	894	19	101
WZD-4-19	148	88	0.60	0.0653	0.0021	1.1023	0.0178	0.1225	0.0018	745	10	782	15	754	9	101
WZD-4-20	250	163	0.65	0.0843	0.0026	2.5944	0.0388	0.2232	0.0032	1299	17	1299	13	1299	11	100
WZD-4-21	54	68	1.25	0.0717	0.0024	1.4090	0.0255	0.1424	0.0021	858	12	979	17	893	11	104
WZD-4-22	135	83	0.62	0.0670	0.0021	1.2726	0.0204	0.1378	0.0020	832	11	836	15	834	9	100
WZD-4-23	135	179	1.32	0.0652	0.0021	1.1536	0.0181	0.1283	0.0018	778	10	782	15	779	9	100
WZD-4-24	98	50	0.51	0.0735	0.0023	1.7376	0.0275	0.1716	0.0025	1021	14	1026	14	1023	10	100
WZD-4-25	197	243	1.24	0.1429	0.0054	7.5518	0.2548	0.3834	0.0065	2092	30	2262	67	2179	30	108
WZD-4-26	117	111	0.94	0.0798	0.0025	2.1962	0.0342	0.1995	0.0029	1173	15	1193	14	1180	11	102
WZD-4-27	276	227	0.83	0.0751	0.0024	1.7416	0.0267	0.1681	0.0024	1002	13	1072	14	1024	10	107

(*continued on next page*)

Table 2 (*continued*)

Samples spot #	U (ppm)	Th (ppm)	Th/U	Isotopic ratio						Age/Ma						Conc. (%)
				$^{207}Pb/^{206}Pb$	±1σ	$^{207}Pb/^{235}U$	±1σ	$^{206}Pb/^{238}U$	±1σ	$^{206}Pb/^{238}U$	±1σ	$^{207}Pb/^{206}Pb$	±1σ	$^{207}Pb/^{235}U$	±1σ	
WZD-4-28	291	209	0.72	0.0856	0.0027	2.6994	0.0410	0.2287	0.0033	1328	17	1329	13	1328	11	100
WZD-4-29	306	90	0.29	0.1463	0.0034	7.7685	0.1373	0.3852	0.0056	2101	26	2303	40	2205	16	110
WZD-4-30	300	164	0.55	0.0696	0.0023	1.4869	0.0438	0.1550	0.0024	929	13	916	70	925	18	100
WZD-4-31	254	178	0.70	0.0818	0.0026	2.3903	0.0367	0.2118	0.0031	1238	16	1242	13	1240	11	100
WZD-4-32	457	117	0.26	0.0721	0.0022	1.6429	0.0250	0.1652	0.0024	986	13	989	14	987	10	100
WZD-4-33	246	227	0.92	0.1097	0.0034	4.8545	0.0743	0.3210	0.0047	1794	23	1794	13	1794	13	100
WZD-4-34	392	389	0.99	0.1062	0.0033	4.2641	0.0649	0.2912	0.0043	1647	21	1735	13	1686	13	105
WZD-4-35	199	70	0.35	0.0625	0.0020	0.9334	0.0151	0.1084	0.0016	663	9	690	15	669	8	101
WZD-4-36	114	102	0.90	0.1667	0.0052	10.9259	0.1665	0.4751	0.0070	2506	31	2525	12	2517	14	101
WZD-4-37	214	69	0.32	0.0709	0.0022	1.5546	0.0244	0.1590	0.0023	951	13	954	14	952	10	100
WZD-4-38	42	35	0.83	0.0725	0.0024	1.3398	0.0259	0.1339	0.0020	810	12	1001	18	863	11	107
WZD-4-40	419	349	0.83	0.0654	0.0031	1.1836	0.0534	0.1313	0.0022	795	12	786	103	793	25	100
WZD-4-41	344	202	0.59	0.0901	0.0028	2.9493	0.0451	0.2374	0.0035	1373	18	1427	13	1395	12	104
WZD-4-42	138	156	1.12	0.0642	0.0034	1.1054	0.0561	0.1250	0.0021	759	12	746	116	756	27	100
WZD-4-43	405	164	0.40	0.0722	0.0022	1.4944	0.0232	0.1502	0.0022	902	12	990	14	928	9	103
WZD-4-44	29	46	1.60	0.0783	0.0028	1.5293	0.0367	0.1416	0.0023	854	13	1155	24	942	15	110
WZD-4-45	224	116	0.52	0.0720	0.0024	1.6735	0.0480	0.1685	0.0026	1004	14	987	68	998	18	99

to those for sample WZD-1 except for slight differences in age cluster distribution for the Archean (Figs. 5 and 7). The zircon population of sample WZD-2 shows the following age peaks: 700–400 Ma, 1300–700 Ma, 1900–1800 Ma and 2500–2400 Ma. Plotted on a probability diagram, maxima in the frequency distribution occur at 957, 1081 and 2440 Ma. Three zircon grains constitute a 1500–1300 Ma age group. The oldest grain has an age of 3418 ± 10 Ma.

4.2. Hanjiadian Group samples WZD-3 and WZD-4

Most zircons collected from the samples WZD-3 and WZD-4 are subhedral to rounded, with most grains less than 100 μm long, showing oscillatory zoning (Fig. 4). Most of the zircons have high Th/U ratios (>0.1) and were likely derived from igneous rocks.

The zircon ages for both samples (Figs. 6 and 7; Table 2) are quite similar. Eighty-six grains from sample WZD-3 yielded a spectrum spanning ages between 437 ± 6 Ma and 3404 ± 10 Ma. The majority of zircons in sample WZD-3 yielded ages between 700 Ma and 1300 Ma with peak ages at 834 Ma and 1009 Ma. There are also minor age groups ranging from 400 Ma to 700 Ma, 1700 Ma to 1800 Ma, and 2400 Ma to 2600 Ma. Three grains have older ages of 3200 Ma, 3240 Ma, and 3400 Ma. The 400–700 Ma group is scattered, defining a peak at about 546 Ma. The 2600–2400 Ga group cluster closely and define a peak at 2501 Ma. The youngest zircon is dated at 437 ± 6 Ma.

Forty-three zircon grains from WZD-4 were analyzed, of which 31 analyses yielded concordant ages of 1400–700 Ma with a peak age at 827 Ma (Figs. 6 and 7). Six grains yielded older ages of 2530–2260 Ma and the four youngest zircon grains have ages of 700–500 Ma. In addition, there are also two analyses with ages of about 1800–1700 Ma.

5. Discussion

5.1. Source rocks for the WZD bauxite

The underlying Hanjiadian Group has been suggested to be the major source rocks for the bauxites because of similar chondrite-normalized REE patterns and ratios of immobile elements (e.g., Jin et al., 2009; Gu et al., 2011). However, it is difficult to ascertain the immobile elements because fractionation of major, trace, and REE elements during bauxitization may have occurred. The Cr–Ni plot indicates that the origin of the WZD bauxite ores is complex and they may not be derived from one single precursor rocks (e.g. Gu et al., 2011). Therefore, it is difficult to identify the source rock from which the bauxite was derived via geochemical investigation.

The zircon ages obtained (Figs. 5–7; Tables 1 and 2) are similar in the four samples studied with some slight differences for the percent of post-Cambrian ages found. From the U–Pb ages of the detrital zircons, we suggest the bauxite and the Hanjiadian Group share a similar provenance. The 120–680 m thick Hanjiadian Group is present throughout the WZD area and it can also be transformed into bauxite through in situ lateritization (Jin et al., 2009). We can conclude that the bauxites were mainly derived from the Hanjiadian Group.

5.2. Provenance of the Hanjiadian Group and bauxite

Though we believe that the source rocks for the WZD bauxite are the Hanjiadian Group, the depositional source of the Hanjiadian Group itself is ill defined because of many cycles of erosion and transportation. Therefore, identification of the provenance of the bauxite and the Hanjiadian Group are necessary to reveal the

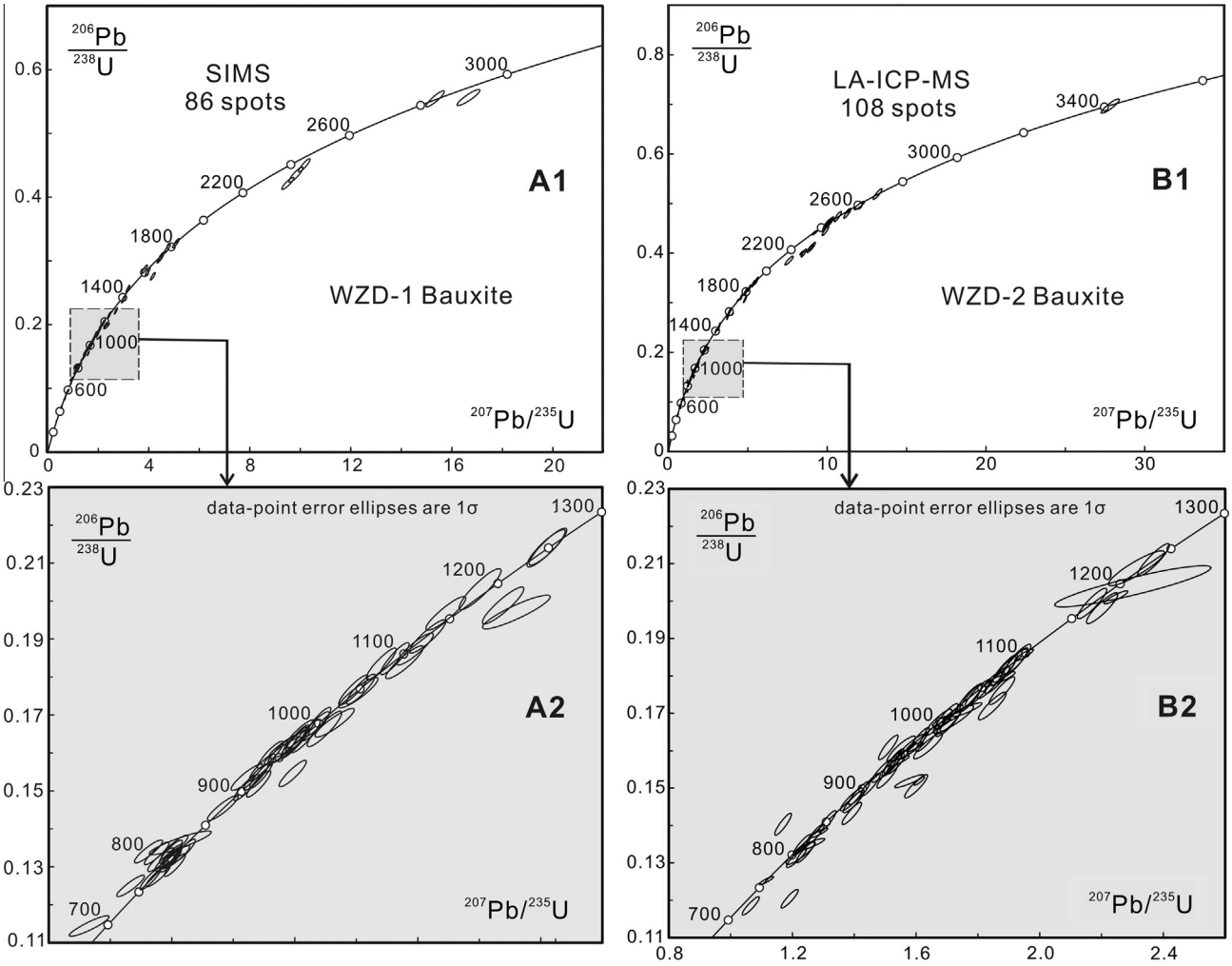

Fig. 5. U–Pb concordia plots of zircon grains from samples of bauxite ores (WZD-1 and WZD-2). Concordia plots A1 and B1 show all analyses. Concordia plots A2 and B2 show the largest age population of zircon grains (0.7–1.3 Ga).

details of the ore-forming process. The age distribution of detrital zircons indicates that the zircons are probably derived from a variety of sources including Neoproterozoic, Mesoproterozoic, Paleoproterozoic, Archean rock units with a minor contribution from Paleozoic rocks. Four main age peaks are evident in the detrital zircon populations of the studied samples: 2600–2400 Ma, 1900–1700 Ma, 1300–700 Ma and 700–400 Ma (Figs. 5–7). The ages of igneous rocks in the basement of the Yangtze Block and Cathaysia Block are summarized in Fig. 7 (Li et al., 2003a, 2003b; Qiu and Gao, 2000; Wang et al., 2006; Zhou et al., 2002b; Li et al., 2002a; Li, 1997; Xiong et al., 2009; Yu et al., 2009). Comparison of age populations helps to identify the sources of the bauxite and the Hanjiadian Group.

All the samples share a common dominant age population ranging from 1300 to 700 Ma (Figs. 5–7). These dominant concordant ages are consistent with previous estimates of late Mesoproterozoic to Neoproterozoic tectonic events at the southwestern margin of the Yangtze Block, such as subduction-related magmatic activity at ca. 1000–740 Ma along the western margin of the Yangtze Block (Sun et al., 2009) and the global Grenville orogenic events at ca. 1300–1000 Ma, owing to the convergence of the Rodinia supercontinent (Hoffman, 1991), suggesting that rocks of this age might have been a major sediment source. Neoproterozoic igneous rocks ranging in age from ca. 1000 Ma to ca. 740 Ma are widespread in the western Yangtze Block (Li et al., 2002a; Zhou et al., 2002b). For instance, the ca. 950–900 Ma Xixiang basalts (Ling et al., 2003) and the ca. 820–740 Ma mafic–ultramafic intrusions in the Hannan region (Zhou et al., 2002a; Zhao and Zhou, 2009), the ca. 890–870 Ma mafic to intermediate plutons (Xiao et al., 2007) and ca. 840–770 Ma volcanic rocks in the Bikou area (Yan et al., 2004), the ca. 860 Ma dioritic Guandaoshan pluton (Sun and Zhou, 2008) and the ca. 810 Ma Gaojiacun and Lengshuiqing mafic–ultramafic intrusive pluton (Shen et al., 2003; Zhou et al., 2006) in the Yanbian region, and the ca. 740 Ma Panzhihua gabbroic intrusion (Zhao and Zhou, 2007) and the ca. 760 Ma Datian adakitic pluton (Zhao and Zhou, 2007). All these Neoproterozoic igneous rocks would be capable of providing sediment for the Hanjiadian Group. Grenville-aged igneous rocks are rarely exposed in the Yangtze Block, whereas rocks of that age are abundant in the Cathaysia Block. In the assembly models of the Rodinia supercontinent (Li et al., 2002b; Yu et al., 2008), those adjacent blocks could be potentially possible regions for these Grenvillian zircons. Rocks with precise Grenvillian U–Pb ages in the Cathaysia Block are the Jingnan rhyolites occurring in the southwestern Wuyi Mountains, which were dated at 972 ± 8 Ma by the SHRIMP U–Pb zircon method, with inherited magmatic zircons dated at ca. 1104–1055 Ma (Shu et al., 2008a,b). In addition, some Grenville-aged detrital/inherited zircons have been found in meta-sedimentary rocks on Hainan Island and northern Fujian (Li et al., 2002b;Wan et al., 2007) and in the Guzai granodiorite in eastern Guangdong (Ding et al., 2005). Therefore, a very large population of Grenville-age zircons may have been available from the igneous rocks of the southern Cathaysia.

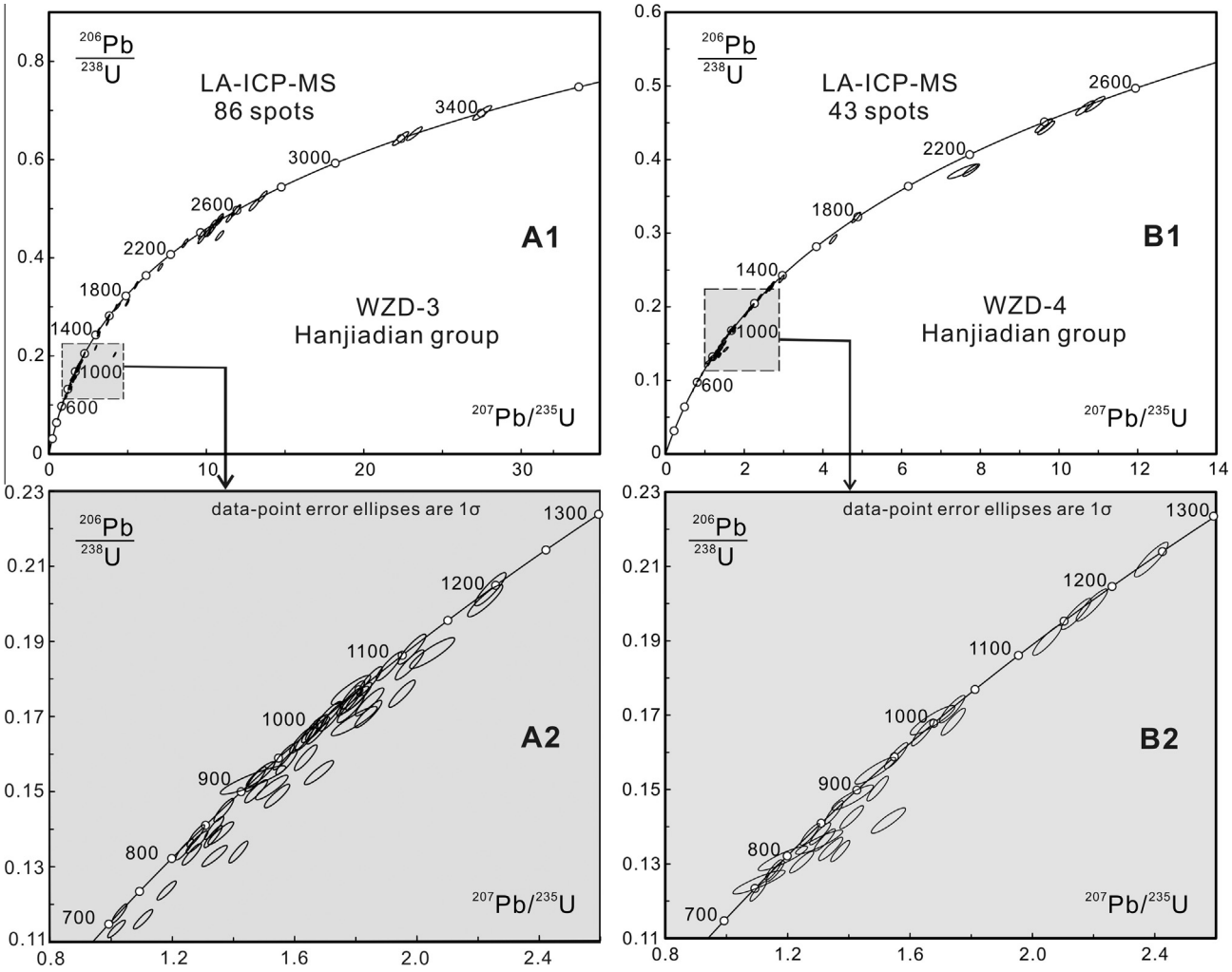

Fig. 6. U–Pb concordia plots of zircon grains from samples of Hanjiadian Group (WZD-3 and WZD-4). Concordia plots A1 and B1 show all analyses. Concordia plots A2 and B2 show the largest age population of zircon grains (0.7–1.3 Ga).

The smaller age population ranging from 1900 Ma to 1700 Ma is consistent with previous estimates of the main episodes of crustal growth in the western Yangtze Block (Li et al., 1991; Sun et al., 2008b, 2009) and the Cathaysia Block (Yao et al., 2011). Zircons with ages of ca. 1800 Ma were obtained from many localities within the both blocks, e.g. the granites (ca. 1854 Ma) in the Kongling terrane (Li, 1997; Li et al., 2010a,b, 2012), the Danzhu gneissic granite (ca. 1854 Ma) in the northern Cathaysia Block (Li and Li, 2007), and the Tianjingping amphibolite (ca. 1766 Ma) in the southwestern Wuyi Mountains (Li, 1997). The detrital zircons with ages of 1900–1700 Ma have also been found in the Meso-Neoproterozoic sedimentary rocks distributed along the western margin of the Yangtze Block (Greentree et al., 2006). Thus, these earlier Meso-proterozoic terranes within the Yangtze Block and Cathaysia Block are likely to be a provenance of the Hanjiadian Group and bauxite. The age histogram indicates an important older age population ranging from 2600 Ma to 2400 Ma (Figs. 5–7). Similar zircon U–Pb ages (2493 ± 19 Ma) for the gneiss from the Yangtze Block have been reported by Tu et al. (2001). The magmatic zircons with similar ages (ca. 2300–2500 Ma) have been found in the basement of the Yangtze Block, but are absent in that of the Cathaysia Block (Greentree et al., 2006). Therefore, a portion of the detrital zircon grains in the Hanjiadian Group and bauxite might have been derived from the earlier paleoproterozoic provenance in the Yangtze Block. A very small population of older detrital zircons (>3000 Ma) found in this study suggests a minor contribution from the Kongling Complex (3200–2900 Ma) exposed on the Yangtze Block. The presence of some younger zircons (700–400 Ma), does not allow us to rule out the contribution of reworked late Neoproterozoic to Ordovician sedimentary sequences.

Above detrital zircons provenance analysis of the Hanjiadian Group and bauxite indicates that their source rocks are dominantly the Neoproterozoic igneous rocks (1000–740 Ma) in the western Yangtze Block and the Grenville-age igneous rocks (1300–1000 Ma) in the southern Cathaysia Block. The Kongling terrane in the northern part of the Yangtze block, the earlier paleoproterozoic terranes within the Yangtze Block, and the earlier Meso-proterozoic terranes within the Yangtze Block and the Cathaysia Block are likely to be additional potential sediment provenance. Although many bauxitic–lateritic deposits are now known within the WZD area, the potential for discovery of additional bauxite deposits remains high in several unexplored districts. These include the central and north Guizhou and west Guangxi districts in the Yangtze Block and some areas in the Cathaysia Block with geology similar to the areas studied for this work.

5.3. Implications for the ore-forming process

Based on LA-ICP-MS and SIMS U–Pb dating of detrital zircons, we propose the following model for bauxite ore formation in the WZD area:

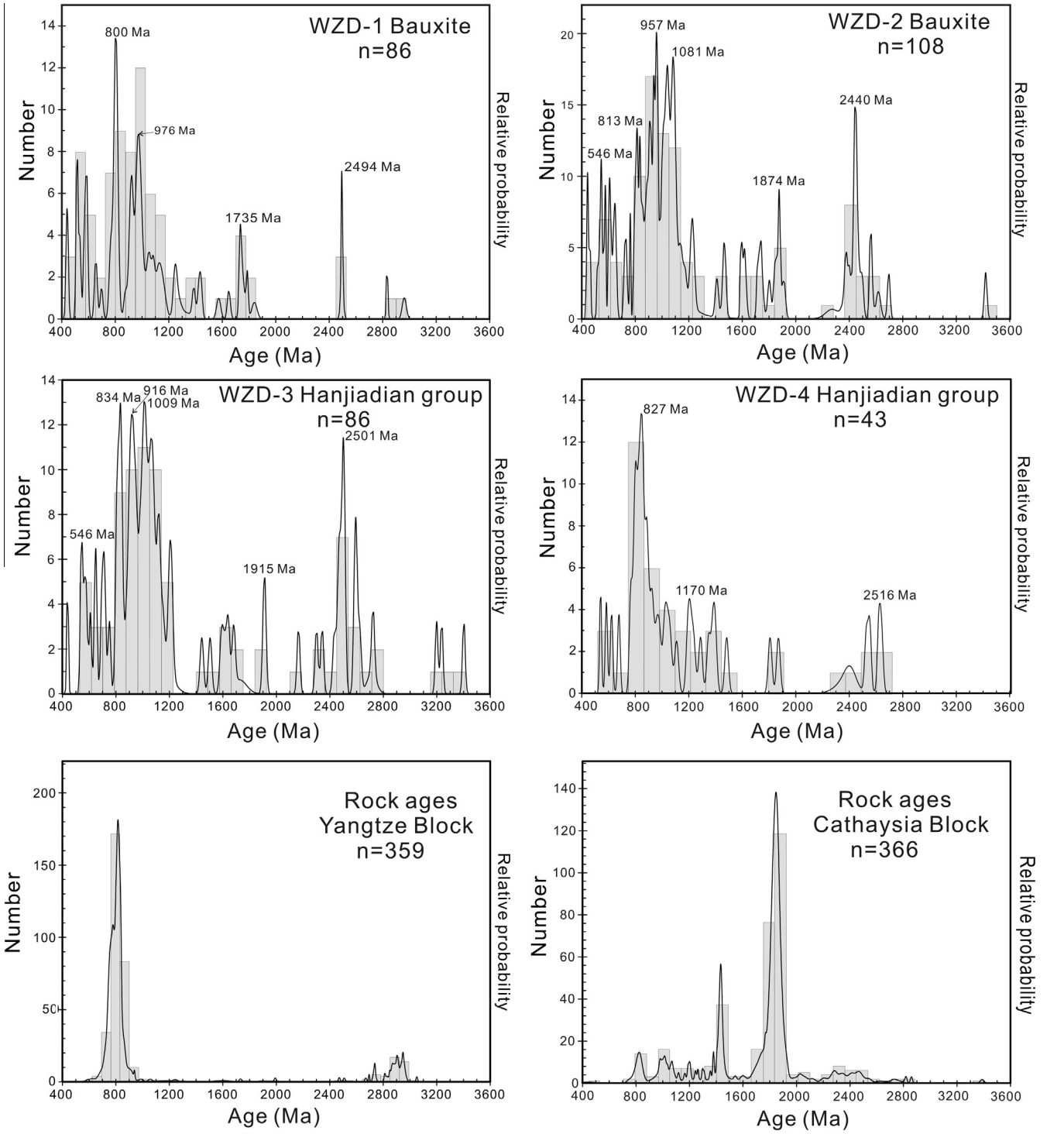

Fig. 7. Probability density plots comparing U–Pb ages for detrital zircon in this study with rock ages in the Yangtze Block (Li et al., 2003a, 2003b; Qiu and Gao, 2000; Wang et al., 2006; Zhou et al., 2002) and Cathaysia Block (Li et al., 2002a; Li, 1997; Xiong et al., 2009; Yu et al., 2009).

Grenville orogenic events (1300–1000 Ma) and the subduction-related magmatic activity along the western edge of the Yangtze Block (1000–740 Ma) caused crustal uplift that exposed associated magmatic rocks and the Precambrian basement rocks. During this period of uplift, the Precambrian basement and magmatic rocks underwent a long periods of intense weathering. Primary minerals (feldspar, ferromagnesians and heavy minerals, etc.) in these rocks were weathered to kaolinite, sericite, quartz, and small amounts of calcite, chlorite, hematite, goethite, rutile, anatase and amorphous materials. Thereafter, the region experienced a large transgressive–regressive cycle from Cambrian to Middle Silurian, resulting in the deposition of weathered material in the Yangtze Block to form Cambro-Ordovician carbonate rocks and the Hanjiadian Group. During the Upper Silurian to Upper Carboniferous, a fall in sea level led to an epeirogenic phase and the subaerial exposure of the Hanjiadian Group and resulting in ceasing of sedimentation. At the same time, the Hanjiadian Group, already enriched in alumina and iron, was subjected to lateritic weathering under subtropical

to tropical climate conditions and thick in situ weathering zones formed. During this early stage of the lateritic weathering, alkalies were leached from the system by acidic solutions, while insoluble elements such as Al, Ti, Fe and Si were reprecipitated as simple oxides and and hydroxides, resulting in the accumulation of bauxitic materials, Fe and Ti oxides, and clay minerals. During the following transgression in the latest Carboniferous, the Huanglong limestone was discontinuously deposited only in the low-lying areas of the Hanjiadian Group. In situ weathering zones developed on the Hanjiadian Group with a probable gentle topography under warm humid climate conditions during the Lower to Middle Permian. At that time, the weathered bauxitic materials were slightly uplifted and subjected to severe lateritic weathering again resulting in the formation of the WZD bauxite deposits. Bauxitic–lateritic horizons were subsequently preserved by deposition of limestone of the Qixia and Maokou Formations and other sediments.

6. Conclusions

LA-ICP-MS and SIMS U–Pb dating of detrital zircons from the bauxite deposits in the WZD area are reported for the first time. The data provide information on the origin of the bauxite, and give new insights into bauxite ore-forming processes.

(1) The similar detrital zircons age patterns suggest that the bauxites may have a close genetic relationship with the underlying Hanjiadian Group. The weathered Hanjiadian Group was partly converted to bauxite by means of progressive in situ lateritic weathering.
(2) The ages of detrital zircons of the bauxite and the Hanjiadian Group from the WZD area compared with the ages of the igneous rocks in the basement of the Yangtze Block and Cathaysia Block indicates that both the Yangtze Block and the Cathaysia Block provide deposipional source for the bauxite and the Hanjiadian Group. The Neoproterozoic igneous rocks (1000–740 Ma) in the western Yangtze Block and the Grenville-aged igneous rocks (1300–1000 Ma) in the southern Cathaysia Block are likely the main provenances of the bauxite and the Hanjiadian Group.
(3) U–Pb dating of detrital zircons indicate that the formation of the bauxite deposits in the WZD area was related to subduction-related magmatic activity along western margin of the Yangtze Block (1.0–0.74 Ga) and the worldwide Grenville orogenic events (1.3–1.0 Ga).

Acknowledgments

We appreciate the assistances of Q.L. Li, Y. Liu, G.Q. Tang, and H. Tao in SIMS dating, X.M. Liu for LA-ICP-MS analyses. The paper has benefited from review comments of the chief editor Bor-ming Jahn and two anonymous reviewers chief editor and two reviewers. This work is jointly supported by the 12th Five-Year Plan project of State Key Laboratory of Ore-deposit Geochemistry, Chinese Academy of Sciences (No. SKLODG-ZY125-02) and the Key Research Program of the Chinese Academy of Sciences (No. KZCX2-YW-Q04-05).

References

Andersen, T., 2002. Correction of common lead in U–Pb analyses that do not report Pb-204. Chemical Geology 192, 59–79.
Bárdossy, G., 1982. Karst bauxites, bauxite deposits on carbonate rocks. Developments in Economic Geology 14, 1–441.
Bárdossy, G., Aleva, G.J.J., 1990. Lateritic Bauxites. Developments in Economic Geology, vol. 27. Elsevier, Amsterdam.
Bárdossy, G., Kovács, Ó., 1995. A multivariate statistical and geostatistical study on the geochemistry of allochtonous karst bauxite deposits in Hungary. Natural Resources Research 4, 138–153.
Boulange B, M.J.P., 1990. Behaviour of the rare earth elements in a lateritic bauxite from syenite (Bresil). Geochemistry of the Earth's Surface and of Mineral Formation 2, 350–351.
Calagari, A.A., Abedini, A., 2007. Geochemical investigations on Permo-Triassic bauxite horizon at Kanisheeteh, east of Bukan, West-Azarbaidjan, Iran. Journal of Geochemical Exploration 94, 1–18.
Chen, Y., Wang, S., Yang, W., 1987. The geological age of Al-bearing rock system and its features of sedimentary facies in Northern Guizhou. Geology of Guizhou 3, 323–338 (in Chinese with English abstract).
Deng, J., Wang, Q., Yang, S., Liu, X., Zhang, Q., Yang, L., Yang, Y., 2010. Genetic relationship between the Emeishan plume and the bauxite deposits in Western Guangxi, China: constraints from U–Pb and Lu–Hf isotopes of the detrital zircons in bauxite ores. Journal of Asian Earth Sciences 37, 412–424.
Ding, X., Zhou, X., Sun, T., 2005. The episodic growth of the continental crustal basement in South China. Geology Review 51, 382–392 (in Chinese with English abstract).
Esmaeily, Dariush, Rahimpour-Bonab, H., Esna-Ashari, A., Alikananian, 2010. Petrography and geochemistry of the Jajarm Karst Bauxite ore deposit, NE Iran: implications for source rock material and ore genesis. Turkish Journal of Earth Sciences 19, 267–284.
Fan, H.P., Zhu, W.G., Li, Z.X., Zhong, H., Bai, Z.J., He, D.F., Chen, C.J., Cao, C.Y., 2013. Ca. 1.5 Ga mafic magmatism in South China during the break-up of the supercontinent Nuna/Columbia: the Zhuqing Fe–Ti–V oxide ore-bearing mafic intrusions in western Yangtze Block. Lithos. http://dx.doi.org/10.1016/j.lithos.2013.02.004.
Fedo, C.M., Sircombe, K.N., Rainbird, R.H., 2003. Detrital zircon analysis of the sedimentary record. In: Hanchar, J.M., Hoskin, P.W.O. (Eds.), Zircon, pp. 277–303.
Gan, X., Li, H., Sun, D., Jin, W., Zhao, F., 1995. A geochronological study on early Proterozoic granitic rocks, southwestern Zhejiang. Acta Petrologica Mineral 14, 1–8 (in Chinese with English abstract).
Greentree, M.R., Li, Z.X., Li, X.H., Wu, H., 2006. Late Mesoproterozoic to earliest Neoproterozoic basin record of the Sibao orogenesis in western South China and relationship to the assembly of Rodinia. Precambrian Research 151, 79–100.
Gu, J., Huang, Z., Jin, Z., Xiang, X., 2011. Immobile elements geochemistry and mass balance calculate of bauxite in Wuchuan–Zheng'an–Daozhen area, Northern Guizhou Province, China. Acta Mineralogica Sinica 31, 397–405 (in Chinese with English abstract).
Guizhou Provincial Geological Survey Bureau, 1987. The Regional Geology of Guizhou province. Geological Publishing House, Beijing, pp. 1–632 (in Chinese with English abstract).
Hao, J., Du, D., Wang, Y., Liu, Y., Gong, H., Ren, J., 2007. A study on sedimentary age of allite formation in North of Guizhou. Acta Mineralogica Sinica 27, 466–472 (in Chinese with English abstract).
Hoffman, P.F., 1991. Did the breakout of Laurentia turn Gondwanaland inside-out? Science 252, 1409–1412.
Horbe, A.M.C., da Costa, M.L., 1999. Geochemical evolution of a lateritic Sn–Zr–Th–Nb–Y–REE-bearing ore body derived from apogranite: the case of Pitinga, Amazonas – Brazil. Journal of Geochemical Exploration 66, 339–351.
Hu, X., 1994. Geochronology of lower Proterozoic Badu Group, southwestern Zhejiang Province. Geochimica 23 (Suppl.), 18–24 (in Chinese with English abstract).
Hu, X., Xu, J., Tong, Z., Chen, C., 1991. The Precambrian Geology of Southwestern Zhejiang Province. Geol. Publish. House, Beijing, pp. 1–278 (in Chinese).
Jiang, Y., Sun, M., Zhao, G., Yuan, C., Xiao, W., Xia, X., Long, X., Wu, F., 2011. Precambrian detrital zircons in the Early Paleozoic Chinese Altai: their provenance and implications for the crustal growth of central Asia. Precambrian Research 189, 140–154.
Jiao, W., Wu, Y., Yang, S., Peng, M., Wang, J., 2009. The oldest basement rock in the Yangtze Craton revealed by zircon U–Pb age and Hf isotope composition. Science in China Series D: Earth Sciences 52, 1393–1399.
Jin, Z., Wu, G., Huang, Z., Bao, M., Zhou, J., 2009. The geochemical chareacteristics of wachangping bauxite deposite in Wuchuan County, Guizhou Province, China. Acta Mineralogica Sinica 29, 458–462 (in Chinese with English abstract).
Karadag, M.M., Kupeli, S., Aryk, F., Ayhan, A., Zedef, V., Doyen, A., 2009. Rare earth element (REE) geochemistry and genetic implications of the Mortas bauxite deposit (Seydisehir/Konya – Southern Turkey). Chemie Der Erde-Geochemistry 69, 143–159.
Li, X.H., 1997. Timing of the Cathaysia Block formation: constraints from SHRIMP U–Pb zircon geochronology. Episodes 20, 188–192.
Li, Z.X., Li, X.H., 2007. Formation of the 1300-km-wide intracontinental orogen and postorogenic magmatic province in Mesozoic South China: a flat-slab subduction model. Geology 35, 179–182.
Li, X.H., Zhao, Z.H., Gui, X.T., Yu, J.S., 1991. Sm–Nd isotopic and zircon U–Pb constraints on the age of formation of the Precambrian crust in Southeast China. Geochimica 3, 255–264 (in Chinese with English abstract).
Li, X.H., Li, Z.X., Zhou, H., Liu, Y., Kinny, P.D., 2002a. U–Pb zircon geochronology, geochemistry and Nd isotopic study of Neoproterozoic bimodal volcanic rocks in the Kangdian Rift of South China: implications for the initial rifting of Rodinia. Precambrian Research 113, 135–154.
Li, Z.X., Li, X.H., Zhou, H.W., Kinny, P.D., 2002b. Grenvillian continental collision in south China: new SHRIMP U–Pb zircon results and implications for the configuration of Rodinia. Geology 30, 163–166.

Li, X.H., Li, Z.X., Ge, W., Zhou, H., Li, W., Liu, Y., Wingate, M.T.D., 2003a. Neoproterozoic granitoids in South China: crustal melting above a mantle plume at ca. 825 Ma? Precambrian Research 122, 45–83.
Li, Z.X., Li, X.H., Kinny, P.D., Wang, J., Zhang, S., Zhou, H., 2003b. Geochronology of Neoproterozoic syn-rift magmatism in the Yangtze Craton, South China and correlations with other continents: evidence for a mantle superplume that broke up Rodinia. Precambrian Research 122, 85–109.
Li, W.X., Li, X.H., Li, Z.X., 2005. Neoproterozoic bimodal magmatism in the Cathaysia Block of South China and its tectonic significance. Precambrian Research 136, 51–66.
Li, X.H., Li, Z.X., Sinclair, J.A., Li, W.X., Carter, G., 2006. Revisiting the "Yanbian Terrane": implications for Neoproterozoic tectonic evolution of the western Yangtze Block, South China. Precambrian Research 151, 14–30.
Li, X.H., Liu, Y., Li, Q.L., Guo, C.H., Chamberlain, K.R., 2009. Precise determination of Phanerozoic zircon Pb/Pb age by multicollector SIMS without external standardization. Geochemistry Geophysics Geosystems 10, Q04010.
Li, X.H., Li, W.X., Wang, X.-C., Li, Q.L., Liu, Y., Tang, G.Q., Gao, Y.Y., Wu, F.Y., 2010a. SIMS U–Pb zircon geochronology of porphyry Cu–Au–(Mo) deposits in the Yangtze River Metallogenic Belt, eastern China: magmatic response to early Cretaceous lithospheric extension. Lithos 119, 427–438.
Li, Z.X., Li, X.H., Wartho, J.A., Clark, C., Li, W.X., Zhang, C.L., Bao, C., 2010b. Magmatic and metamorphic events during the Early Paleozoic Wuyi-Yunkai Orogeny, southeastern South China: new age constraints and P–T conditions. Geological Society of America Bulletin 122, 772–793.
Li, X.H., Li, Z.X., He, B., Li, W.X., Li, Q.L., Gao, Y., Wang, X.C., 2012. The Early Permian active continental margin and crustal growth of the Cathaysia Block: in situ U–Pb, Lu–Hf and O isotope analyses of detrital zircons. Chemical Geology 328, 195–207.
Liaghat, S., Hosseini, M., Zarasvandi, A., 2003. Determination of the origin and mass change geochemistry during bauxitization process at the Hangam deposit, SW Iran. Geochemical Journal 37, 627–637.
Liang, T., 1989. Mineralization geological conditions and mechanism problems of bauxite deposits of the North part of Guizhou province. Acta Sedimentologica Sinica 7, 57–67 (in Chinese with English abstract).
Liao, S.F., 1988. The geological times of the bauxite strata of palaeoresiduum facies in Guizhou and the problems in contrast with Southern Sichuan, Western Hunan and Western Hubei. Geology of Guizhou 5, 342–348 (in Chinese with English abstract).
Ling, W.L., Gao, S., Zhang, B.R., Li, H.M., Liu, Y., Cheng, J.P., 2003. Neoproterozoic tectonic evolution of the northwestern Yangtze craton, South China: implications for amalgamation and break-up of the Rodinia Supercontinent. Precambrian Research 122, 111–140.
Liu, P., 1995. On the bauxite in Guizhou Province-V: the bauxite-bearing rock series in Central Guizhou-Southern Sichuan ore-forming zone. Geology of Guzhou 12, 185–203 (in Chinese with English abstract).
Liu, P., 2007. Bauxite geology in the Wuchuan–Zhengan–Daozhen area, Northern Guizhou. Geology and Prospecting 43, 29–33 (in Chinese with English abstract).
Liu, X., Wang, Q., Deng, J., Zhang, Q., Sun, S., Meng, J., 2010a. Mineralogical and geochemical investigations of the Dajia Salento-type bauxite deposits, western Guangxi, China. Journal of Geochemical Exploration 105, 137–152.
Liu, Y., Xia, Y., Wang, J., 2010b. Metallogenic characteristics and metallogenic factors of bauxite deposits in Northern Guizhou. Bulletin of Mineralogy Petrology and Geochemistry 29, 422–425 (in Chinese with English abstract).
Long, X., Yuan, C., Sun, M., Xiao, W., Zhao, G., Wang, Y., Cai, K., Xia, X., Xie, L., 2010. Detrital zircon ages and Hf isotopes of the early Paleozoic flysch sequence in the Chinese Altai, NW China: new constrains on depositional age, provenance and tectonic evolution. Tectonophysics 480, 213–231.
Ludwig, K.R., 2003. ISOPLOT 3.0: a Geochronological Toolkit for Microsoft Excel. Berkeley Geochronology Center. Special Publication No. 4, pp. 1–71.
MacLean, W.H., Bonavia, F.F., Sanna, G., 1997. Argillite debris converted to bauxite during karst weathering: evidence from immobile element geochemistry at the Olmedo Deposit, Sardinia. Mineralium Deposita 32, 607–616.
Mutakyahwa, M.K.D., Ikingura, J.R., Mruma, A.H., 2003. Geology and geochemistry of bauxite deposits in Lushoto District, Usambara Mountains, Tanzania. Journal of African Earth Sciences 36, 357–369.
Najman, Y., 2006. The detrital record of orogenesis: a review of approaches and techniques used in the Himalayan sedimentary basins. Earth-Science Reviews 74, 1–72.
Newson, T., Dyer, T., Adam, C., Sharp, S., 2006. Effect of structure on the geotechnical properties of bauxite residue. Journal of Geotechnical and Geoenvironmental Engineering 132, 143–151.
Peng, M., Wu, Y.B., Wang, J., Jiao, W.F., Liu, X.C., Yang, S.H., 2009. Paleoproterozoic mafic dyke from Kongling terrain in The Yangtze Craton and its implication. Chinese Science Bulletin 54, 1098–1104.
Peng, M., Wu, Y.B., Gao, S., Zhang, H.F., Wang, J., Liu, X.C., Gong, H.J., Zhou, L., Hu, Z.C., Liu, Y.S., Yan, H.L., 2012. Geochemistry, zircon U–Pb age and Hf isotope compositions of Paleoproterozoic aluminous A-type granites from the Kongling terrain, Yangtze Block: constraints on petrogenesis and geologic implications. Gondwana Research 22, 140–151.
Pereira, M.F., Linnemann, U., Hofmann, M., Chichorro, M., Sola, A.R., Medina, J., Silva, J.B., 2012. The provenance of Late Ediacaran and Early Ordovician siliciclastic rocks in the Southwest Central Iberian Zone: constraints from detrital zircon data on northern Gondwana margin evolution during the late Neoproterozoic. Precambrian Research 192–195, 166–189.
Qiu, Y.M.M., Gao, S., 2000. First evidence of >3.2 Ga continental crust in the Yangtze craton of South China and its implications for Archean crustal evolution and Phanerozoic tectonics. Geology 28, 11–14.
Schwarz, T., 1997. Lateritic bauxite in central Germany and implications for Miocene palaeoclimate. Palaeogeography, Palaeoclimatology, Palaeoecology 129, 37–50.
Shen, W.Z., Gao, J.F., Xu, S.J., Tan, G.Q., Yang, Z.S., Yang, Q.W., 2003. Age and geochemical characteristics of the Lengshuiqing body, Yanbian, Sichuan Province. Acta Petrologica Sinica 19, 27–37 (in Chinese with English abstract).
Shu, L.S., Deng, P., Yu, J.H., Wang, Y.B., Jiang, S.Y., 2008a. The age and tectonic environment of the rhyolitic rocks on the western side of Wuyi Mountain, South China. Science in China (D) 38 (8), 950–959.
Shu, L.S., Faure, M., Wang, B., Zhou, X.M., Song, B., 2008b. Late Paleozoic–early Mesozoic geological features of South China: response to the Indosinian collision event in Southeast Asia. Comptes Rendus Geosciences 340, 151–165.
Sun, W.H., Zhou, M.F., 2008. The ~860-Ma, Cordilleran-type Guandaoshan dioritic pluton in the Yangtze Block, SW China: implications for the origin of Neoproterozoic magmatism. The Journal of Geology 116, 238–253.
Sun, M., Chen, N., Zhao, G., Wilde, S.A., Ye, K., Guo, J., Chen, Y., Yuan, C., 2008a. U–Pb Zircon and Sm–Nd isotopic study of the Huangtuling granulite, Dabie-Sulu belt, China: implication for the Paleoproterozoic tectonic history of the Yangtze Craton. American Journal of Science 308, 469–483.
Sun, W.H., Zhou, M.F., Yan, D.P., Li, J.W., Ma, Y.X., 2008b. Provenance and tectonic setting of the Neoproterozoic Yanbian Group, western Yangtze Block (SW China). Precambrian Research 167, 213–236.
Sun, W.H., Zhou, M.F., Gao, J.F., Yang, Y.H., Zhao, X.F., Zhao, J.H., 2009. Detrital zircon U–Pb geochronological and Lu–Hf isotopic constraints on the Precambrian magmatic and crustal evolution of the western Yangtze Block, SW China. Precambrian Research 172, 99–126.
Taylor, G., Eggleton, R.A., Foster, L.D., Tilley, D.B., Le Gleuher, M., Morgan, C.M., 2008. Nature of the Weipa Bauxite deposit, northern Australia. Australian Journal of Earth Sciences 55, S45–S70.
Tu, Y.J., Yang, X.Y., Zheng, Y.F., Li, H.M., 2001. Zircon U–Pb age of the gneiss from southeastern Anhui. Acta Petrologica Sinica 17 (1), 157–160 (in Chinese with English abstract).
Wan, Y.S., Liu, D.Y., Xu, M.H., Zhuang, J., Song, B., Shi, Y., Du, L., 2007. SHRIMP U–Pb zircon geochronology and geochemistry of metavolcanic and metasedimentary rocks in Northwestern Fujian, Cathaysia Block, China: tectonic implications and the need to redefine lithostratigraphic units. Gondwana Research 12, 166–183.
Wang, X.L., Zhou, J.C., Qiu, J.S., Zhang, W.L., Liu, X.M., Zhang, G.L., 2006. LA-ICP-MS U–Pb zircon geochronology of the Neoproterozoic igneous rocks from Northern Guangxi, South China: implications for tectonic evolution. Precambrian Research 145, 111–130.
Wang, L.J., Griffin, W.L., Yu, J.H., O'Reilly, S.Y., 2012. U–Pb and Lu–Hf isotopes in detrital zircon from Neoproterozoic sedimentary rocks in the northern Yangtze Block: implications for Precambrian crustal evolution. Gondwana Research. http://dx.doi.org/10.1016/j.gr.2012.04.013.
Wiedenbeck, M., Alle, P., Corfu, F., Griffin, W.L., Meier, M., Oberli, F., Vonquadt, A., Roddick, J.C., Speigel, W., 1995. Three natural zircon standards for U–Th–Pb, Lu–Hf, trace element and REE analyses. Geostandards Newsletter 19, 1–23.
Wu, G., Liu, Y., Zhang, Y., 2006. Geological characters and aluminum ore resources potential in the Wuchuan–Zhengan–Daozhen area. Guizhou Geology and Prospecting 42, 39–43 (in Chinese with English abstract).
Wu, G., Jin, Z., Bao, M., Mao, Z., 2008a. Bauxite metallogenic regularity in the Wuchuan–Zhengan–Daozhen area, Northern Guizhou. Geology and Prospecting 44, 31–35 (in Chinese with English abstract).
Wu, Y.B., Zheng, Y.F., Gao, S., Jiao, W.F., Liu, Y.S., 2008b. Zircon U–Pb age and trace element evidence for Paleoproterozoic granulite-facies metamorphism and Archean crustal rocks in the Dabie Orogen. Lithos 101, 308–322.
Xiao, L., Zhang, H.-F., Ni, P.-Z., Xiang, H., Liu, X.-M., 2007. LA-ICP-MS U–Pb zircon geochronology of early Neoproterozoic mafic-intermediat intrusions from NW margin of the Yangtze Block, South China: implication for tectonic evolution. Precambrian Research 154, 221–235.
Xiong, Q., Zheng, J., Yu, C., Su, Y., Tang, H., Zhang, Z., 2009. Zircon U–Pb age and Hf isotope of Quanyishang A-type granite in Yichang: signification for the Yangtze continental cratonization in Paleoproterozoic. Chinese Science Bulletin 54, 436–446.
Yan, Q., Hanson, A.D., Wang, Z., Druschke, P.A., yan, Z., Wang, T., Liu, D., Song, B., Jian, P., Zhou, H., Jiang, C., 2004. Neoproterozoic Subduction and Rifting on the Northern Margin of the Yangtze Plate, China: implications for Rodinia reconstruction. International Geology Review 46, 817–832.
Yao, J., Shu, L., Santosh, M., 2011. Detrital zircon U–Pb geochronology, Hf-isotopes and geochemistry—new clues for the Precambrian crustal evolution of Cathaysia Block, South China. Gondwana Research 20, 553–567.
Yin, K., 2009. Mineralization and metallogenic model for bauxite in the Wuchuan–Zheng'an–Daozhen area, Northern Guizhou. Acta Sedimentologica Sinica 27, 452–457 (in Chinese with English abstract).
Yu, J.H., Zhou, X., O'Reilly, S.Y., Zhao, L., Griffin, W.L., Wang, R., Wang, L., Chen, X., 2005. Formation history and protolith characteristics of granulite facies metamorphic rock in Central Cathaysia deduced from U–Pb and Lu–Hf isotopic studies of single zircon grains. Chinese Science Bulletin 50 (18), 2080–2089.
Yu, J.H., O'Reilly, S.Y., Wang, L., Griffin, W.L., Zhang, M., Wang, R., Jiang, S., Shu, L., 2008. Where was South China in the Rodinia supercontinent? Evidence from

U–Pb geochronology and Hf isotopes of detrital zircons. Precambrian Research 164, 1–15.
Yu, J.H., Wang, L., O'Reilly, S.Y., Griffin, W.L., Zhang, M., Li, C., Shu, L., 2009. A Paleoproterozoic orogeny recorded in a long-lived cratonic remnant (Wuyishan terrane), eastern Cathaysia Block, China. Precambrian Research 174, 347–363.
Yu, J.H., O'Reilly, S.Y., Wang, L., Griffin, W.L., Zhou, M.F., Zhang, M., Shu, L., 2010. Components and episodic growth of Precambrian crust in the Cathaysia Block, South China: evidence from U–Pb ages and Hf isotopes of zircons in Neoproterozoic sediments. Precambrian Research 181, 97–114.
Yu, J.H., O'Reilly, S.Y., Zhou, M.F., Griffin, W.L., Wang, L., 2012. U–Pb geochronology and Hf–Nd isotopic geochemistry of the Badu Complex, Southeastern China: implications for the Precambrian crustal evolution and paleogeography of the Cathaysia Block. Precambrian Research 222–223, 424–449.
Yuan, H.L., Gao, S., Dai, M.N., Zong, C.L., Guenther, D., Fontaine, G.H., Liu, X.M., Diwu, C., 2008. Simultaneous determinations of U–Pb age, Hf isotopes and trace element compositions of zircon by excimer laser-ablation quadrupole and multiple-collector ICP-MS. Chemical Geology 247, 100–118.
Zarasvandi, A., Charchi, A., Carranza, E.J.M., Alizadeh, B., 2008. Karst bauxite deposits in the Zagros Mountain Belt, Iran. Ore Geology Reviews 34, 521–532.
Zarasvandi, A., Zamanian, H., Hejazi, E., 2010. Immobile elements and mass changes geochemistry at Sar-Faryab bauxite deposit, Zagros Mountains, Iran. Journal of Geochemical Exploration 107, 77–85.
Zhang, S.B., Zheng, Y.F., Wu, Y.B., Zhao, Z.F., Gao, S., Wu, F.Y., 2006a. Zircon isotope evidence for $\geqslant$3.5 Ga continental crust in the Yangtze Craton of China. Precambrian Research 146, 16–34.
Zhang, S.B., Zheng, Y.F., Wu, Y.B., Zhao, Z.F., Gao, S., Wu, F.Y., 2006b. Zircon U–Pb age and Hf–O isotope evidence for Paleoproterozoic metamorphic event in South China. Precambrian Research 151, 265–288.
Zhang, S.B., Zheng, Y.F., Wu, Y.B., Zhao, Z.F., Gao, S., Wu, F.Y., 2006c. Zircon U–Pb age and Hf isotope evidence for 3.8 Ga crustal remnant and episodic reworking of Archean crust in South China. Earth and Planetary Science Letters 252, 56–71.
Zhao, X., Wang, T., 2008. Bauxite deposits in Wulong–Nanchuan, Chongqing: characteristics and ore potential. Sedimentary Geology and Tethyan Geology 28, 110–112.
Zhao, J.H., Zhou, M.F., 2007. Geochemistry of Neoproterozoic mafic intrusions in the Panzhihua district (Sichuan Province, SW China): implications for subduction-related metasomatism in the upper mantle. Precambrian Research 152, 27–47.
Zhao, J.H., Zhou, M.F., 2009. Secular evolution of the Neoproterozoic lithospheric mantle underneath the northern margin of the Yangtze Block, South China. Lithos 107, 152–168.
Zhao, X.F., Zhou, M.F., Li, J.W., Sun, M., Gao, J.F., Sun, W.H., Yang, J.H., 2010. Late Paleoproterozoic to early Mesoproterozoic Dongchuan Group in Yunnan, SW China: implications for tectonic evolution of the Yangtze Block. Precambrian Research 182, 57–69.
Zheng, J.P., Griffin, W.L., O'Reilly, S.Y., Zhang, M., Pearson, N., Pan, Y.M., 2006. Widespread Archean basement beneath the Yangtze craton. Geology 34, 417–420.
Zhou, M.F., Kennedy, A.K., Sun, M., Malpas, J., Lesher, C.M., 2002a. Late Proterozoic arc-related mafic intrusions along the northern margin of South China: implications for the accretion of Rodinia. The Journal of Geology 110, 611–618.
Zhou, M.F., Yan, D.P., Kennedy, A.K., Li, Y., Ding, J., 2002b. SHRIMP U–Pb zircon geochronological and geochemical evidence for Neoproterozoic arc-magmatism along the western margin of the Yangtze Block, South China. Earth and Planetary Science Letters 196, 51–67.
Zhou, M.F., Ma, Y., Yan, D.P., Xia, X., Zhao, J.H., Sun, M., 2006. The Yanbian Terrane (Southern Sichuan Province, SW China): a Neoproterozoic arc assemblage in the western margin of the Yangtze Block. Precambrian Research 144, 19–38.
Zhuang, J., Huang, Q., Deng, B., 2000. Strata Subdivision and Petrology of Precambrian Metamorphic Rocks in Fujian. Xiamen University Press, Xiamen, pp. 80–90 (in Chinese).